NASA CR-72742

CASE FILE
COPY

INVESTIGATION OF ADVANCED REGENERATIVE
THRUST CHAMBER DESIGNS

By

V. R. Stubbs

AEROJET LIQUID ROCKET COMPANY

Prepared For

NATIONAL AERONAUTICS AND SPACE ADMINISTRATION

NASA LEWIS RESEARCH CENTER
CONTRACT NAS 3-7971
R. A. DUSCHA, PROJECT MANAGER

FINAL REPORT

INVESTIGATION OF ADVANCED REGENERATIVE
THRUST CHAMBER DESIGNS

By

V. R. Stubbs

AEROJET LIQUID ROCKET COMPANY
Sacramento, California

Prepared For

NATIONAL AERONAUTICS AND SPACE ADMINISTRATION

November 15, 1970

CONTRACT NAS 3-7971

NASA LEWIS RESEARCH CENTER
CLEVELAND, OHIO

R. A. Duscha, Project Manager

NOTICE

Requests for copies of this report should be referred to

National Aeronautics and Space Administration
Scientific and Technical Information Facility
P. O. Box 33
College Park, Md. 20740

FOREWORD

The work presented herein was performed for NASA/LeRC under Contract NAS 3-7971 titled "Investigation of Advanced Regenerative Thrust Chamber Designs". Mr. R. A. Duscha was the NASA/LeRC project manager.

The author wishes to acknowledge contributions by V. E. Kahle for the section on vapor deposition of tungsten and J. A. Cunningham and J. W. Starr for the heat transfer and stress studies reported under Task V. The heat transfer studies reported under Task IV were performed by Messrs. A. C. Kobayashi and R. L. Ewen.

Mr. V. R. Stubbs, the author of this report, was Program Manager of the subject program.

TABLE OF CONTENTS

TABLE LIST

FIGURE LIST

FIGURE LIST

ABSTRACT

A regeneratively cooled thrust chamber has been fabricated with a vapor deposited tungsten flame liner, a plasma sprayed tungsten-zirconia thermal barrier, and an electroformed nickel coolant jacket with integrally formed coolant channels. The fabrication processes are described and illustrated. Additionally, off-design thermal analyses and startup and shutdown transient analyses are presented for a nominal 400 psia P_c, 8000 lb thrust, F_2/H_2 engine.

I.   SUMMARY

        The objective of Contract NAS 3-7971 was the analytical and mechanical
design and fabrication of a regeneratively cooled fluorine/hydrogen thrust
chamber incorporating a refractory flame liner, a thermal barrier, and
electroformed nickel channels.

        Task I, reported previously in NASA CR 72266 (Reference 1), was concerned
with design and heat transfer, stress and fabrication analysis. During Task
II, a thrust chamber was fabricated which followed the design and fabrication
concept developed during Task I. The initial fabrication step was to construct
a graphite mandrel incorporated a 2.375-in.-dia steel shaft; this shaft was
utilized as the basic axis to which all subsequent diametral dimensions were
held. This graphite mandrel was then wrapped with tungsten screen, preparatory
to being tungsten coated using a vapor deposition process. A vapor deposition
tank was fabricated which used a welding positioner as the mandrel rotating
mechanism and quartz lamps to heat the mandrel. The quartz lamp infrared
heating system was unsatisfactory due to the tendency of HF and other reaction
products to etch the quartz window of the tank. High frequency induction
heating was also unsatisfactory due to the local excess heating of the
tungsten screen used as the nucleating surface. Satisfactory results were
obtained with Cal-Rods imbedded in the graphite, although area heat control
was more difficult than with the previous methods.

        Following vapor deposition of the tungsten, a gradated tungsten-zirconia
thermal barrier coating was applied by plasma-arc spraying. Design dimensions
for the coating were not held due to tolerance buildup. Rather than attempt
to grind the coating back to print tolerance, the drawings were changed to
incorporate the "as-built" dimensions. The coated mandrel was then sent to
the Linde Division of Union Carbide where a 0.003 to 0.005 in. thick nickel
coating was applied by the detonation gun process. The nickel coating was
required to provide a conductive surface for the subsequent nickel electro-
forming operation.

        Camin Laboratories Inc., Brooklyn, New York, did the electroforming
and related machining. The inner shell is generated by electroforming a layer
of nickel on the mandrel and machining it to the desired thickness and contour.
Coolant passages are formed by machining the ribs into a vinyl filler material,
"growing" the ribs by electroforming and machining to contour. The vinyl is
replaced with a meltable wax before electroforming the outer jacket. The
wax is removed by melting and chemical cleaning. Details of this process,
which results in integrally formed coolant channgels, are proprietary.
Problems were encountered obtaining a smooth finish while machining the
vinyl core material. Additionally, excessive pressure drop was recorded in
water flow testing. It is not known whether the ΔP variation was related
to electroforming or to subsequent machining and welding operations.

        The fabrication of the thrust chamber was completed at Aerojet, where a
machining error in the divergent nozzle area necessitated rework by welding,
electroforming, and machining. Following the repair, leakage was evident when
the chamber was tested at 760 psig with water. The major leaks were repaired

I, Summary (cont.)

by removing the flame liner and thermal barrier over 4.0 in. of axial length
measured from the exit plane. An additional thickness of nickel was electro-
formed over the discrepant areas. Remaining leaks were considered minor.
Leakage did not occur with water at 500 psig although air bubbles were evident
when Leak-Tek was applied.

Subsequent flow testing revealed an unexplainably high pressure drop with
ambient water at 15 lb/sec flow rate. On the assumption that there might be
electroforming core material remaining in the coolant channels, the unit was
vacuum dehydrated and flowed with trichlorethylene and MEK. Although slight
improvement was noted in retesting, the pressure drop was still approximately
three times the predicted value. There is no confirmed explanation for the
disparity between the actual and calculated values. After the cleaning efforts,
a considerable increase in leakage rate was evident, indicating that foreign
material may have been removed from the leak passages.

Task III, Thrust Chamber Plumbing, provided for the design, fabrication,
and assembly of inlet and outlet plumbing conforming to the NASA/LeRC test
facility requirements. This task was completed routinely. Pressure drop in the
plumbing was determined to be 17 psig.

Task IV, Off-Design Thermal Analyses, considered the thermal effect of
three off-design steady-state test firing conditions. Increasing the coolant
flow rate 25 and 50% had no significant effect on the tungsten flame liner
temperature, although the nickel interface temperatures were reduced approxi-
mately 200 and 300°F, respectively. The greatest reduction in wall temperatures
occurs under conditions of P_c = 300 psia and MR = 8.0, at which the tungsten wall
temperature is reduced from 4590°F maximum to 3460°F and the nickel interface
temperature is reduced from 1520°F maximum to 1060°F. The results of these
analyses are considered in the recommended startup and shutdown conditions and
procedures described in the Task V section of this report.

Task V, Startup and Shutdown Transient Analysis, consisted of thermal and
stress analyses to determine the effects of various startup and shutdown pro-
cedures. Although it was determined that margins of safety were adequate under
conditions of a step function start, the temperature gradients and therefore
the stresses are reduced with a ramp start. A 2- to 3-sec ramp start incorporating
a fuel lead and a step function shutdown with fuel TCV closing following the
oxidizer TCV closing by 0.075 sec are recommended.

2

II.   INTRODUCTION

Various fabrication methods have been investigated in recent years for applicability to the construction of high pressure, high heat flux, regeneratively cooled liquid rocket engine thrust chambers. The brazed tube bundle constructions have performed well; however, the brazed tube bundle method involves expensive, and time-consuming techniques such as tube tapering, die forming, hand assembly of tubes, and often hand brazing to repair discrepancies following the furance brazing. Because of the high tooling cost, the thrust chamber design is not easily changed to accommodate new inventions or changes of nozzle contour, coolant passage size, or area ratio.

The objective of this program was to investigate new fabrication methods and design techniques having potential for recuding fabrication time and cost, reducing heat flux to the coolant, and increasing thrust chamber life. Design requirements were that it be nontubular and meet the following nominal engine specifications:

Thrust	8000 lb
Chamber pressure	400 psia
Oxidizer	Fluorine
Fuel	Hydrogen
Mixture ratio F_2/H_2	12
Nozzle expansion ratio	60
Characteristic length	25.0 in. minimum
Nozzle length	38.910 in. maximum
Coolant inlet pressure	675 psia
Coolant outlet pressure	550 psia
Coolant inlet temperature	50°R
Chamber diameter	5.390 in.
Throat diameter	3.843 in.
Injector interface	NASA Dwg CD 620831

As noted, the results of Task I were reported in Reference 1. The results of Tasks II through V are reported in this, the final report. The subsequent program tasks were as follows:

Task II, Thrust Chamber Fabrication, included completion of detailed component design, fabrication of the thrust chamber, and pressure and flow testing of the thrust chamber.

Task III, Thrust Chamber Plumbing, required the design and fabrication of inlet and outlet plumbing suitable to the NASA/LeRC test facility.

Task IV, Off-Design Thermal Analysis, was an investigation of three off-design steady-state thermal conditions to provide data for the planning of a thrust chamber test program.

II, Introduction (cont.)

Task V, Startup and Shutdown Transient Analysis, required the performance of heat transfer and stress analyses with the objective of determining an acceptable startup and shutdown cycle for thrust chamber testing.

III. TASK II - CHAMBER FABRICATION

A. GENERAL

The fabrication and design analyses performed under Task I of the program resulted in selection of a final design, certain fabrication processes, and a fabrication plan. Figure 1 illustrates the final design configuration and materials. The nozzle extension was not fabricated. Briefly, the processes and the sequence of fabrication selected are as follows:

A graphite mandrel was constructed with a 2-3/8-in.-dia pipe center (Fig. 2). Tungsten screen was then wrapped on the graphite mandrel and tungsten was vapor deposited on the assembly to a depth of 0.030 in. Next, a gradated tungsten-zirconia thermal barrier was plasma sprayed over the screen. This was surrounded by an electroformed nickel jacket with integral coolant channels. Components such as the injector and aft flange and the inlet and outlet manifolds were welded to the electroformed nickel using the electron beam method. Finish machining was followed by pressure and flow checking.

The following sections describe in detail the fabrication steps outlined above. This is followed by recommendations for process and design changes to avoid the problems experienced.

B. TUNGSTEN. VAPOR DEPOSITION

1. The Reaction

The chemical vapor plating of tungsten is a reduction process whereby the halide of the metal is reduced by hydrogen to form metallic tungsten and HF, according to the following reaction:

$$WF_{6(g)} + 3H_{2(g)} \xrightarrow{heat} W_{(s)} + 6HF_{(g)}$$
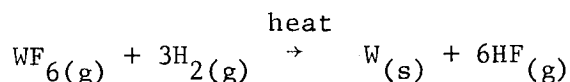
The reaction occurs at the heated surface of a substrate, with the metal condensing on the surface and the other reaction product, HF, passing off as a gas.

The primary deposition-rate-controlling parameter is temperature, with the deposition reaction beginning at 392°F and the rate increasing with temperature. Although other investigators have plated at 1200°F and above, it was found in an Aerojet-sponsored research program that surface finish and thickness are easier to control at lower temperatures. At 650°F, the deposit is smooth, having only a few nodules, and the thickness is uniform.

Aerojet-sponsored experiments also established that graphite is an excellent substrate and that nucleation is greatly accelerated by use of a tungsten screen surrounding the graphite. G-90 graphite was selected as the mandrel material because its thermal expansion closely matches that of tungsten at the 650°F temperature.

III, B, Chemical Vapor Deposition (cont.)

2. Equipment and General Procedure

a. Heating System Selection

Induction heating, several methods of resistance heating, and the use of an infrared lamp system were evaluated as methods for heating the graphite mandrel 650°F. The infrared lamp concept was initially chosen for the following reasons:

(1) Simplicity of Design - No expensive power source equipment would be needed as is required for induction heating. The limited space for bringing power leads to the rotating mandrel and the need for a rotating power pickup are objections to the use of resistance or induction heating. Repairs to the infrared heating unit could be made without stopping the test run.

(2) Safety - In case of an oxygen leak, there would be no ignition source in the chamber as there would be with induction or resistance heating.

(3) Control - With individually controlled lamps, the temperature along the length of the substrate could be closely controlled.

b. Original Approach - Infrared Heating

The entire chemical vapor deposition chamber and rotating mechanism was located in a large spark-proof Bink's hood. The water-cooled chamber used for the plating was 31 in. in diameter and 40 in. high. The graphite mandrel was placed on a turntable inside the plating chamber which was then sealed to exclude air and moisture. Figure 2 shows the graphite mandrel mounted on the rotating mechanism, with the water-cooled chamber suspended beside it. The tube configuration visible through the window is the plating manifold. The mandrel was rotated at about 5 rpm during plating to ensure an even coating. Heat was provided by a bank of quartz infrared lamps (Figure 3) placed outside the chamber and focused on the substrate through a quartz window. The lamps were individually controlled to allow variation of the power input along the length of the substrate. Figure 4 shows the assembled chamber, with the infrared lamps in position, in the Bink's hood. The inside of the chamber is painted with a high-temperature silicone paint for reflectivity. The chamber and the quartz window frame are water cooled to below the lower deposition temperature to prevent tungsten from plating on them. An argon purge tube surrounds the window to provide protection from the reactive gases.

III, B, Chemical Vapor Deposition (cont.)

The substrate temperature was measured using thermocouples placed just below the surface of the graphite. The stainless-steel-sheathed thermocouples were placed in holes in the substrate and the lead wires brought down through the center bore. The tip of the sheathed thermocouple was threaded into a graphite plug. The plugs were cemented into holes in the substrate and then blended with the substrate contour.

The reactive gases were mixed in a mixing tee and a long tube before being introduced into the reaction chamber through a water-cooled manifold. The manifold was shaped to the graphite mandrel's countour, with small holes drilled along the length to distribute the reactive gases on the surface of the substrate. The WF_6 gas was metered by a Brooks Kel-F flow meter and the H_2 gas by a Mathison tubular flow meter. The reactive gas system was redundant, making it possible to clean the lines or make repairs without shutting down.

A cold trap removed the unreacted WF_6 from the exhaust gases, after which the gases are bubbled through a lime solution to neutralize the HF. The exhaust-gas system was also redundant.

The summary of test runs presented in Table I indicates the problem encountered as the quartz window overheated excessively. This problem of overheating resulted in the infrared heating approach being abandoned.

c.   Second Approach - Induction Heating

A 23 KW high frequency induction unit and a pancake-type coil were used as a heat source. The possibility of arcing was minimized by application of an Al_2O_3 coating to the coil (Figure 5). A recirculating cooling system for the induction coil and the gas manifold was also installed. With this system, it was possible to maintain the cooling water temperature within $\pm 20°F$. Induction heating proved to be infeasible due to overheating of any portion of the tungsten screen not in contact with the graphite.

d.   Third Approach - Cal-Rod Resistance Heating

The graphite mandrel was drilled to receive Cal-Rod resistance heating elements. Six heating elements, 13 in. long, were placed 60° apart in the cylindrical forward section, 3/4 in. from the outer surface of the graphite. Two sets of Cal-Rods were placed in the aft section of the mandrel, one set 12 in. long and the other 9 in. long. Each set was wired in series to a separate 45-ampere Variac to provide heat control in three zones.

III, B, Chemical Vapor Deposition (cont.)

An exhaust and scrubber system was designed and installed to provide a more efficient method of neutralizing the HF and also to eliminate plugging of the lines. The gas lines were 1-in.-dia polyvinyl chloride pipe, with 1-in.-dia gate and ball valves. The scrubber system consisted of two liquid injectors which applied a slight vacuum on the exhaust lines by spraying a caustic solution into an aspirator, thereby mixing the neutralizing solution with the exhaust gases. The caustic solution was recirculated from two 50-gal drums and kept neutral or basic by the addition of lime.

3. Summary of the Experimental Runs

Fifteen experiments were made to develop and qualify the method to be used for the vapor deposition of the tungsten. These are presented in Table I.

Experiment Numbers 1 through 6 were made to test the equipment and make alterations as necessary. In Experiment 2, it was found that the design power capability of the infrared lamps was too low. As a result, the chamber was insulated and the 750-watt lamps were replaced by 1000-watt lamps. Other minor design changes made as a result of these tests included changes of gasket material, the addition of a water trap in the exhaust system, and increased rotating clearances between the mandrel shaft and the bearing housing.

After Experiment 7, it was obvious that the provisions for cooling the quartz window were inadequate and a major redesign of the window-cooling system was needed to prevent tungsten from plating on it.

Considering these difficulties, it was decided to try the alternative heating methods described previously. A 25 KW induction unit was installed and a pancake induction coil was designed and tested. The coil, flame sprayed with Al_2O_3 to reduce arcing, is shown in Figure 5 as it appeared after several test runs.

Experiments 8 through 12 were made to evaluate the induction coil and other parts of the system. The system had the disadvantage in that no changes in zone temperatures could be made during a run; a new coil would be needed for each temperature change. It was found that the induction coil would not work with a tungsten-screen-wrapped mandrel. Each time the screen passed underneath the coil, the screen was heated to such a high temperature that parts of it expanded and lifted off the mandrel. Repeated attempts to improve screen-mandrel fit up and attachment were unsuccessful. Since it was unlikely that the screen would bond to the graphite during plating, there would be little control over the plating rate, which is highly dependent upon temperature.

III, B, Chemical Vapor Deposition (cont.)

Since the plating was not considered to be accomplished with induction heating, it was decided to use resistance heating. Cal-Rods were installed in a full-scale graphite mandrel and a rotating power pickup designed and installed. Experiments 13 and 14 provided information which indicated that this approach would work satisfactorily. Separate three-zone controls provide more freedom to control temperature than the induction coil, though it was not as versatile as the quartz lamp system. Experiment 15 proved that, with the proper adjustments in zone temperature, the Cal-Rod heating method would work. Figure 6 shows the power control unit with the three 45-amp Variac control units, the deposition chamber (in position), and the reactive-gas control panel.

4. Discussion of Final Results

a. Preparation of the Graphite Mandrel for Plating

The graphite mandrel and tungsten screen were kept free of contamination during machining and handling. All adhesives, epoxies, and Saureisen cement were eliminated from the system because experience indicated that the tungsten would not deposit on the bond lines. The graphite sections of the mandrel were counterbored and pinned together; the thermocouple-hole plugs were machined to a tight slip fit and hand fitted into the holes.

Several methods of attaching the tungsten screen to the mandrel were considered and a few were tried. Flat patterns were developed for the aft or divergent section, the throat section, and the cylindrical sections. An attempt was made to cut these three sections out of tungsten screen and sew the pieces together with 0.005-in.-dia wire. This method has the advantage of having few seams or places where the screen overlaps. However, use of the sewing technique produced a coarse seam, which was expected to result in a porous structure. Also, the conical section and the throat section pieces of screen could not be pulled tight because parts of the pieces had to be cut on the bias. When screen or cloth was pulled on the bias, it did not become tight but, instead, changed shape.

The spiral wrap method was chosen to cover the mandrel with tungsten screen. A paper pattern was developed by measuring the graphite mandrel at ten stations along the length of the mandrel and drawing smooth curves through these points to form the contour. The paper pattern was then refined until a suitable pattern was developed. Figure 7 is a picture of the tungsten screen covered mandrel.

A second lot of tungsten screen was more difficult to fit than the first lot. Program schedule considerations resulted in the use of the screen as received.

III, B, Chemical Vapor Deposition (cont.)

b. Final Deposition Run

Analysis of the data from Experiment 15 indicated that a plating time of 35 hr was needed to deposit a tungsten coating to the required 0.030-in. thickness. Figure 8 is a photomicrograph taken of the plating deposited on the graphite mandrel and the tungsten screen in Experiment 15.

On the basis of the results of this experiment, the test mandrel was removed and one of the final run mandrels installed. The exhaust system was rebuilt and the final plating run started. One-half hour after starting the plating run, one of the new aspirators malfunctioned and lime solution was drawn into the trap just outside the plating chamber. Some moisture also entered the chamber and caused a slight discoloration of the plated surface. This discoloration caused no difficulty in plating when the run was resumed after the aspirator was repaired. The balance of the 35-hr plating run was completed with only minor difficulties with the new exhaust system.

The coating was bright and metallic at the termination of the plating run but gradually developed grayish-blue color as the cooldown cycle proceeded. This discoloration was easily removed from the surface with a wire brush. The part is illustrated in Figure 9 after plating and before removal of the discoloration. In some areas at the extreme exit section, the screen had lifted from the graphite surface and did not bond. The screen was removed from these areas and the coating blended with plasma-arc sprayed tungsten. The plating on the remainder of the part was of good quality except for one area of porosity midway on the divergent section where the screen strips overlapped slightly. The coating thickness averaged 0.044 in. on the cylindrical portion, 0.045 in. in the throat, and 0.039 in. in the divergent section. A few nodules and areas where the edges of the screen plated heavily were hand ground with a diamond dust wheel. A slight taper in the cylindrical section was eliminated by grinding.

C. THERMAL BARRIER APPLICATION

1. General

The thermal barrier material selected during the Task I study was gradated tungsten-zirconia. The thickness of each layer was determined on the basis of the desired thermal resistance and tailored to minimize thermal gradients. Figure 1 specifies the coating configuration. Plasma-arc spraying was the method selected for coating application. Original planning called for plasma spraying a final layer 0.004 in. of pure nickel. However, after excessive porosity was found in three tests of the plasma-sprayed material, it was decided to employ the Linde detonation gun process for the final conductive layer.

III, C, Thermal Barrier Application (cont.)

2. Plasma Arc Spraying

a. Method

The thrust chamber was coated using the rotation mechanism and hydraulic torch feeding mechanism shown in Figure 10. This equipment was designed for internal spraying of liquid propellant thrust chambers but was adapted to external spraying. A cam duplicating the chamber contour was employed. It was necessary to offset the torch from the boom, however, to clear the exit end diameter and maintain a constant torch-to-workpiece distance. The torch holder boom operated from a feed screw that is controlled to give the selected forward feed per revolution of the chamber. A program was developed to maintain a constant surface speed and a constant feed per revolution. Special tooling consisted of adapter plates to secure the chamber to the large drive wheels and a manifold to carry the LN_2 coolant to the chamber exterior directly below the chamber. Figure 11 shows the chamber midway in the process and Figure 12 shows the chamber when the plasma arc spraying is 90% complete.

b. Results

The plasma arc spraying was completed routinely; however, the wire screen joints or discrepant areas that were evident after vapor deposition appeared somewhat exaggerated after coating. High spots and nodules were filed off by hand, but the contour was not machined because of the possibility that the coating might be damaged.

D. ELECTROFORMING THE COOLANT JACKET

1. Electroforming Process Plan

The results of the Electroform Development subtask of Task I established the requirements and procedure for electroforming the coolant jacket. Camin Laboratories, Inc., was selected as the subcontractor and participated in development of the design. Certain portions of Camin's electroforming process (for example, the methods of cleaning and sensitizing the substrate) are proprietary; however, the general procedure followed by Camin Laboratories is illustrated in Figure 13. This method of "growing" the ribs is covered by a patent granted to Camin Laboratories.

2. Electroforming Results

The actual electroforming was preceded by two added operations: measuring and cleaning. The chamber was measured to establish actual diametral dimensions after the detonation-gun nickel coating and as a check on measurements

III, D, Electroforming the Coolant Jacket (cont.)

taken after plasma arc spraying. There was general agreement on dimensions and the nickel topcoat varied in thickness from 0.002 to 0.005 in. Drawings were changed to conform to the measured dimensions and these were used for the fabrication of tracer templates for contour machining. Camin Laboratories noticed that the nickel topcoat was very difficult to chemically clean; there was excessive bleeding of what appeared to be impurities. After cleaning, however, Camin did not report any difficulty in obtaining a bond.

The electroforming and machining sequence proceeded as planned except in the machining of the vinyl. In cutting the rib slots in the vinyl (see Figure 14), it was found that the cutting speed required to make a smooth, clean cut in vinyl was excessive for cutting the nickel at the bottom of the slot. It had been planned that a few mils of the nickel inner shell would be removed in this operation to leave a clean surface. An additional machining operation at a slower cutting feed and speed was required to cut the nickel. Some mismatch and chatter occurred, resulting in rough rib cavity walls. The photograph in Figure 15 gives some indication of the machining results. As this roughness was duplicated in the nickel, Camin Laboratories was requested to smooth the walls by hand grinding. The actual roughness could not be determined as the channels had already been filled with wax, the process step beyond the planned inspection point, before inspection could be made. The only other discrepancy reported was that the ribs did not form completely, leaving small cracks or grooves along the rib lands. Inspection revealed that these incomplete ribs were prevalent in most of the chamber area. The ribs gave the appearance of having plated adequately on the sides of the cavity but not in the center, with the result that the nickel tended to grow together from each side without bonding in the center. The sketch below illustrates the appearance of the ribs as formed.

1/32 max
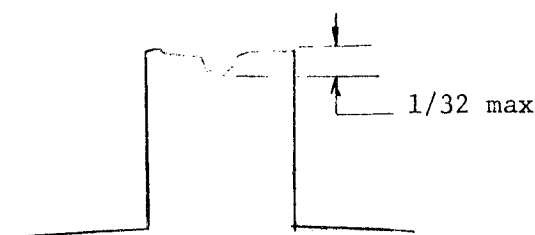
The maximum depth of cavity in the rib was approximately 1/32 in. Because the cavity was discolored and thus might contain impurities, it was agreed that the surface would be removed by hand grinding. Camin Laboratories indicated that, with additional chemical cleaning, the outer shell nickel would bond and fill the cavities.

12

III, D, Electroforming the Coolant Jacket (cont.)

The outer shell was electroformed and machined to final contour. The completed area was masked and the chamber returned to the bath for buildup of the local heavy areas in the throat and at the manifold attachment points. These areas were subsequently machined to final dimensions. The final operation was to remove the wax from the channels by heating the assembly to the melting temperature of the wax and then flowing solvent through the channels to remove any residue. The solvent flow was reported by Camin to have been repeated until no evidence of foreign material was evident in the solvent. The completed chamber was crated and shipped to Aerojet by air on 15 July 1969. The electroforming task of the program had started on 30 April 1968.

E.   THRUST CHAMBER FINAL ASSEMBLY

1.   Mandrel Removal and Inspection

The graphite mandrel was removed from the chamber by machining and hand work. It had been planned to press out the steel pipe center to provide easy access for a boring bar. However, the steel mandrel was frozen in place, evidently due to corrosion or nickel plating solution buildup, and the major portion of the graphite had to be removed before the mandrel could be released.

Figure 16 shows the chamber in a lathe in process of inspection. A maximum diametral eccentricity of 0.0125 in. was found in the exit area. This was presumed to be due to relieving of plating and other stresses on removal of the graphite mandrel. Sufficient stock had been left on the manifold attachment areas of the components to permit match machining to obtain a maximum clearance of 0.004 in. for electron beam welding.

2.   Electron Beam Welding

The electron beam welding was accomplished at the Aerojet Azusa facility. During the welding, excessive outgassing was noted at the lower joint of the inlet manifold to the chamber. Inspection after welding indicated porosity. For this reason, it was decided to machine a U-groove weld preparation and weld with the TIG process with an overlay fillet. A chemical analysis performed on a electroformed nickel specimen from the same solution as the outer shell confirmed that the metal was 99.2% pure nickel, per specification, and contained no sulphur. Welding problems, it was concluded, were due to porosity but not impurities. Figures 17 and 18 illustrate the weld joint design of the inlet manifold and outlet manifold, respectively. Figures 19 and 20 show the chamber in the electron beam vacuum chamber with the welding head in position for welding the inlet manifold joints.

13

III, E, Thrust Chamber Final Assembly (cont.)

3. Thrust Chamber Final Machining

a. Machining Error and Repair

A machining error during final machining of the aft flange resulted in excessive metal being removed from the coolant channel aft closure wall. A spacer ring was machined and welded in place to replace the material removed in error. Some weld cracking was noted at the edge of the weld on the inner wall. Electroforming was investigated as a possible repair procedure and appeared to have an excellent chance for success. The NASA/ LeRC project manager approved this approach. The thrust chamber was sent to Electroforms, Inc., Gardena, California, where electroformed nickel was built up over the discrepant area and approximately 1.0 in. of the chamber inner surface. Figure 21 shows the repaired area after machining.

b. Pressure Tests and Leak Repairs

The chamber was proof tested with water to 1100 psig and leak tested at 760 psig. Leaks were found in what appeared to be four separate areas under the thermal barrier liner. The aft two inches of liner material were removed but no leaks were found in the uncovered area. Subsequent leak tests, during which the water level was gradually lowered and measured on a sight gage, indicated the leaks to be approximately 2.0 in. further upstream. An additional 2.0 in. of liner material was removed and two "major" leaks were located in the area uncovered. At least two "minor" leaks were indicated to be under the liner upstream by formation of minute bubbles when the chamber was pressurized with air at 500 psi. These were considered minor, as no leakage occurred when the water level was raised above the apparent leak location. A layer of nickel was electroformed over the bared area to a depth of 0.040 in. to repair the two visible leaks. This repair was blended to the original repair at the aft end. However, no effort was made to bond the nickel to the thermal barrier liner at the upstream locations as it was considered undesirable to block the escape path of the still-existing minor leaks.

The repair was completed by making a light machine cut over the repaired area and by grinding the aft end of the thermal barrier liner to eliminate the discontinuity. Figure 21 is a photograph taken from the aft end showing the first electroform repair. Figures 22 and 23 are photomicrographs of the holes found in leak testing. Figure 22 shows a single hole having the appearance of the metal bridging over a void. The leak path of the hole, as evidenced by the emitted stream of water, was nearly parallel to the surface. The leak in the area shown in Figure 23 was from the small crack in the center of a small dimple. A considerable amount of scattered porosity can be seen in the area.

III, E, Thrust Chamber Final Assembly (cont.)

c.   Investigation of the Cause of Leaks

It is not possible to make a conclusive determination of the cause of the leaks without destructive testing. However, the following facts are known: (1) the surface of the thermal barrier liner was rough and, although an attempt was made to remove all nodules or protrusions, it is possible that a small local protrusion may have existed; and (2) the detonation gun nickel coating applied over the tungsten-zirconia thermal barrier was very difficult to chemically clean. Camin Laboratories reported black fluid emissions from the surface.

On the basis of fact number (1), it is possible to make the following supposition: a local protrusion resulted in a thin area of the nickel inner shell that failed under the 1100 psig proof load. The appearance of the hole in Figure 23 tends to support this theory.

Based on fact number (2), it can be postulated that the nickel substrate was not continuous, or contained a nonmetallic inclusion, which resulted in the electroformed nickel bridging over the nonconductive area, leaving a void. This void or nonconductive area could have developed during the coating process, however, it is more likely that the detonation gun nickel coating was damaged in handling or transit in a manner that left a small nonconductive area, resulting in bridging, as noted above, and void areas within the nickel.

Although the leak cause cannot be verified, the following recommendations are made to preclude leakage from the possible causes described. First, the substrate contour should be ground to an axi-symmetric configuration to remove all small protrusions left by previous processes. Secondly, the conductive coating applied over the nonconductive substrate should be inspected both visually and by an electric probe arrangement to ensure that the coating is continuous. This inspection should be made immediately prior to electroforming.

d.   Flow Testing

After the major leaks had been repaired as described above, the thrust chamber was flow tested using 15 lb/sec of ambient water with 200 psi back pressure. Pressure drop was recorded to be 403 psi from manifold to manifold. A pressure drop of 108 psi had been analytically predicted. Recalculation of the predicted value indicated a maximum of 156 psi might be expected under the most adverse tolerance and finish conditions. It was concluded that blockage of the chamber had occurred at some stage in the manufacturing process or during the rework plating and machining. Since the manifolds were welded in place, it was impossible to inspect or test individual channels. On the assumption that some of the core material used in the electroforming process

III, E, Thrust Chamber Final Assembly   (cont.)

could be remaining within the coolant channels, the chamber was vacuum dehydrated at 250°F for 12 hr. Inspection after vacuum dehydrating revealed green, powdery material on the chamber inside surface at locations which indicated the material had been sucked out through the existing leak paths under the liner.

Pressure drop did not decrease on a second flow test. The chamber was then flowed with hot trichlorethylene in an attempt to dissolve any remaining core material. Nothing was noted in this operation to indicate that any foreign material was being dissolved and removed. During a delay of 48 hr before the flow test facility became available for a third test, the chamber was filled with methylethyl ketone (MEK). When the MEK was drained, some red plastic or wax was noted under the liner. This was presumed to be the plastic sealant used to seal the liner downstream edge during the final electroform repair.

Subsequent flow testing indicated a reduction in pressure drop of 9.6 psi. During the test, it was noted that the leak rate previously estimated at 20 drops/min at 760 psi had increased considerably. A static pressure test was made and water leakage recorded at 23 cc per min. The photograph (Figure 24), taken after the final repair and leak check, shows the areas of leakage. The flow testing sequence and results are shown in Table II.

The pressure drop at 15 lb/sec flow rate is the average of each test group calculated as follows:

$$\Delta P_t = \left(\frac{lb/sec}{Kw_t}\right)^2$$

where:

$$Ratio = \frac{\Delta H \ Daniels \ Plate}{\Delta P_n \ test}$$

$$Kw_t = K_w \ Daniels \ Plate \ \sqrt{ave \ of \ ratios}$$

$$Kw \ Daniels \ Plate = 1.4081$$

After discussion with the NASA/LeRC project manager, no further efforts were made to determine the cause of the excessive pressure drop. A photographic record was made of the leak locations (Figure 24) and the thrust chamber was crated and shipped to NASA/LeRC, Cleveland, Ohio.

IV.   TASK III - THRUST CHAMBER PLUMBING

This task was completed in November 1969. The work accomplished consisted of design of inlet and outlet plumbing conforming to a sketch and specifications furnished by NASA. Some changes were made for ease of fabrication. The photograph in Figure 25 shows the completed thrust chamber with plumbing welded in place.

V.   TASK IV - OFF-DESIGN STEADY-STATE HEAT TRANSFER ANALYSIS

    A.   INTRODUCTION

        This task required the performance of three off-design steady-state heat transfer analyses. The work was completed in November 1969, at which time the results were presented as an enclosure to the Monthly Progress Report. The computer printout sheets were presented to the NASA project manager at that time.

    B.   METHOD OF ANALYSIS

        The advanced regenerative thrust chamber analyzed (AGC Drawing No. 1146503) consists of a tungsten-zirconia liner with an electroformed nickel shell which contains rectangular coolant channels. The channel dimensions are designed to provide sufficient hydrogen cooling to maintain the coating and channel wall temperatures at reasonable values without excessive coolant pressure drop and, at the same time, to provide strength and ease of fabrication. The coolant channel configuration is a typical 1-1/2 pass design. Two coolant passes are employed in the nozzle from area ratio 6:1 to the exit (16:1), which permits preheating of the low temperature hydrogen. After passing through the two-pass region, the hydrogen flows through the high heat flux throat and combustion chamber zones in a single pass and enters the collection manifold at the injector end of the chamber. The coating thermal resistance is tapered from the coolant inlet to the throat.

        Steady-state heat transfer calculations for this thrust chamber were made for the LF_2/LH_2 operating conditions given in Table III. These conditions were used as input for the analysis in a steady-state regenerative heat transfer program (Reference 2) on the UNIVAC 1108 computer. This program performs local one-dimensional analyses at the coolant channel centerline for various stations along the thrust chamber and calculates wall temperatures, pressure drops, and total heat rejection. It is essentially the same program as used in the analysis of the Titan family and M-1 thrust chambers, and it is currently being used extensively in the analysis of the NERVA nozzles. The one-dimensional analytical procedures employed in the present calculations are essentially the same as those discussed in Reference 1 and, therefore, a detailed description will not be presented herein. However, four changes were made and are described below. In addition, the two-dimensional conduction analyses of Reference 1 were not performed in the present effort.

        The coolant channel surface roughness was increased from 64 micro-inches in Reference 1 to 90 microinches herein, based on the roughness of the actual chamber. A K-factor of 0.9 was used at the tube inlet to account for turning as well as the sudden contraction; a factor of 0.9 was applied to both the inlet and exit velocity heads at the turn-around. At internal enlargements and contractions and at the tube exit, the form loss factors of Reference 1 were used. The net effect of these changes was to reduce the total form loss and give a very slightly lower nominal pressure drop than reported in Reference 1, in spite of the increased surface roughness and frictional pressure drop.

18

V, B, Method of Analysis

For ease of computation, the thermal properties used in calculating the gas-side heat transfer coefficients were evaluated at the arithmetic mean of the recovery temperature and the gas-side wall (coating) temperature instead of at the Eckert reference enthalpy. The resultant change in the heat transfer coefficient was **insignificant** due to the relatively high wall temperatures of the thrust chamber.

The hydrogen coolant heat transfer coefficient for this investigation was based on the experimentally determined Hess and Kunz correlation:

$$h_L = 0.0208 \ C_L \ \frac{K_f}{D_e} \ \left(\frac{\rho_f \ V \ D_e}{\mu_f} \right)^{0.8} \ Pr_f^{0.4} \ \left(1 + 0.01457 \ \frac{\nu_w}{\nu_b} \right)$$

The selection of this correlation was based on Aerojet-General Corporation experience in the NERVA program where thrust chamber test data comparisons were made. An extensive investigation was made of many different correlations with available experimental single-tube heat transfer test data before selecting the Hess and Kunz equation. The report of Reference 3 concluded that the Hess and Kunz film-temperature design equation with a variable CL appears to best represent pertinent single-tube test data for cryogenic hydrogen. As recommended, C_L was varied from 0.85 in the straight tube section to 1.00 in the throat section to account for curvature enhancements. Use of the Hess and Kunz correlation reduced the coolant heat transfer coefficient compared to Reference 1; at the throat, this reduction caused an increase of 140°F in the maximum nickel temperature. A calculation was made to determine the local effects of removing 4.0 in. of the liner at the exit end. It was found that increase in nickel wall temperature was minimal.

C. DISCUSSION OF RESULTS

The results of the present analysis are summarized in Table IV, which also includes the nominal conditions predicted in Reference 1. It must be emphasized that the present results are based on one-dimensional heat transfer across the wall thickness. Axial and circumferential heat conduction resulting from the relatively high thermal conductivity of the nickel coolant channels will result in lower maximum nickel and coolant surface temperatures. The combustion chamber results of Reference 1 include the effects of circumferential conduction, which reduced the maximum nickel temperature by 80°F compared to the corresponding one-dimensional analysis. Therefore, the differences between Reference 1 and the present nominal wall temperatures in the chamber are caused by both two-dimensional effects and the change in coolant heat transfer correlation; at the throat, the differences are due solely to the coolant correlation.

The maximum combustion chamber wall temperatures presented in Table IV occur at the tube split at area ratio -1.45 (axial distance 11.9 in.), as shown by the temperature distributions of Figure 26. However, the nickel-coating interface and coolant-side temperatures following the rib thickness

V, C, Discussion of Results (cont.)

change at axial distance 10.4 in. are essentially the same as those at the tube split. Two heat flux distributions are given in Figure 27; the chamber values given in Table III are at the injector interface. Figure 28 shows the coolant bulk temperature and static pressure distributions for the nominal case.

Table IV indicates that increasing the coolant flow rate has little effect on the coating temperature or the heat flux. This is to be expected since the gas-side flow and the coating dominate the overall thermal resistance. However, the maximum nickel temperature is reduced by 310°F (to 1210°F) when the coolant flow is increased to 150% nominal; the coolant inlet pressure must be increased by 124 psi (to 884 psia) to maintain the outlet pressure at 550 psia.

Reducing chamber pressure to 300 psia and mixture ratio to 8.0 provides much less severe thermal conditions since the gas-side heat transfer coefficient is reduced by almost 25%, the combustion product stagnation temperature is reduced by 1000°F, and the coolant flow is increased by 8%. As a result, the maximum coating temperature is reduced by 1130°F (to 3460°F) from the nominal case, and the maximum nickel temperature is reduced by 460°F (to 1060°F). Therefore, both nickel and coating temperatures are lower than in the case of 150% coolant flow at the nominal chamber pressure and mixture ratio.

All results presented herein could be changed significantly if coolant flow maldistribution occurs due to nonuniform heating or flow resistance or if flow instability occurs. Investigation of these possibilities, which are pertinent for very compressible coolant systems, was not included in this study.

VI.   TASK V - STARTUP AND SHUTDOWN TRANSIENT ANALYSIS

A.   INTRODUCTION

This task required the performance of thermal and stress analyses to identify an acceptable startup and shutdown cycle for thrust chamber testing. The previous structural analysis (Reference 1) which was based on steady-state temperature conditions indicated that the throat section was the critical structural area with regard to its sensitivity to thermally induced loads. The throat area was analyzed for various startup and shutdown combustion transients, including a step function start, a 2-sec ramp start, and a step function shutdown. The design was found to be adequate for any of the transients although it is low cycle fatigue limited.

B.   METHOD OF ANALYSIS

Using a thermal model modified from the Task I steady-state analyses (Reference 1), a parametric thermal study was made, permitting inspection of the data to determine (1) the thermal gradients in relation to the steady-state predictions, and (2) the selection of the critical areas for further analysis.

The thermal model consisted of a two-dimensional node network which was solved in turn at 18 chamber locations, beginning at the coolant inlet and ending at the injector. The local changes in chamber and thermal barrier geometry were included as were local changes in the gas-side heat transfer coolant pressure and temperature. The coolant bulk temperature rise was calculated using the average heat flux between chamber stations. The coolant pressure drop calculation used average coolant properties and a rough channel friction factor. Figure 29 shows the thermal model node network. For illustration, a computer printout sheet showing typical input and output data is shown in Figure 30.

The stress analyses employed the detailed finite element program used during Task I for the steady-state analysis and for the step function shutdown analysis. In this study, steady-state temperatures were used with $P_c = 0$. Figure 31 shows a computer plot of the grid.

From the steady-state analysis in Task I and inspection of the parametric thermal analysis data, it was found that the throat area is the shutdown, a gross finite element representation of the computer model was utilized. A computer plot of this grid is shown in Figure 32. This analytical approach provided a relative comparison of stresses for thermal transients; also, the method required a minimal imput of nodal point temperature data as a function of time and accounted for plasticity of materials.

VI, Task V -- Startup and Shutdown Transient Analysis (cont.)

C.   SUMMARY OF RESULTS

The finite element analysis of the throat region for a step function shutdown condition was conducted in detail to determine the stress distribution at the coolant channel. The analysis assumed the chamber pressure instantly equal to zero and the coolant channel pressure remaining at 730 psi. The results of this analysis did not significantly vary from the steady-state analysis results. The minimum margin of safety for the nickel shell increased from +0.60 to +1.1 and the maximum compressive hoop strain in the tungsten increased from 1.2% to 1.32%.

Analyses of the throat section for a step function start, a 2-sec ramp start, and a step function shutdown were conducted. A comparison of the results to the steady-state thermal analysis showed that these start and shutdown conditions did not produce excessive stresses and are acceptable operating procedures. However, the transient thermal conditions produced slightly higher compressive stresses in the tungsten and tungsten zirconia and tensile stresses in the nickel than during steady state. Tensile stresses in the nickel were well within allowable values.

D.   CONCLUSIONS

1.   The finite element analysis of the throat section for a step function shutdown at time equal zero showed there was a negligible change in stress conditions with immediate reduction of chamber pressure ($P_c = 0$).

2.   The transient conditions of both startup and shutdown subject the tungsten and tungsten-zirconia to a greater compressive hoop strain than calculated for steady state. This makes the chamber low cycle fatigue limited. Further finite element analysis and a low cycle fatigue analysis would be needed to determine the limiting number of cycles anticipated.

3.   Although the analysis performed indicates that a step function start is acceptable, prudence dictates that, if the equipment capability exists, a 2- or 3-sec ramp start be adopted. A modified step function shutdown as noted in the analysis section is recommended. It is also recommended, based on the results of the off-design study (Task IV), that the first test firing be at MR = 8 and P_c = 300 psi.

E.   THERMAL ANALYSIS

1.   Combustor Cycles

In order to establish the effect of combustor transients on wall thermal stresses, five startup combustion cycles and two shutdown combustion cycles were investigated as follows:

VI, E, Thermal Analysis (cont.)

Startup

1. P_C = 400 psia, stepped startup

2. P_C = 400 psia, 0.3 sec linear P_C ramp

3. P_C = 300 psia, stepped start

4. P_C = 400 psia, 2.0 sec linear P_C ramp

5. P_C = 400 psia, 3.0 sec stepped ramp

Shutdown

1. P_C = 400 psia, stepped shutdown

2. P_C = 400 psia, 0.3 sec linear ramp

These seven startup and shutdown combustion cycles are shown schematically in Figure 33.

2. Parametric Studies

The thermal stress in the W/ZrO$_2$ thermal barrier may be expressed as a function of the temperature drop in the thermal barrier and is proportional to ΔT.

$$\sigma \sim \Delta T$$

Another meaningful temperature parameter is the average barrier temperature, $\bar{T}$, since the mechanical properties of the barrier, such as Young's modulus and yield strength, are all functions of $\bar{T}$.

Two plots are shown on Figure 34. The first shows ΔT vs $\bar{T}$ for the W/ZrO$_2$ coating at the throat. This curve may be used to estimate the W/ZrO$_2$ stress level at a particular $\bar{T}$. The curves for the second plot were obtained by cross-plotting the P_C = 400 ramped startup curves from the ΔT vs $\bar{T}$ plot. A study of these curves lead to the following conclusions:

The dashed curve clearly shows that the thermal stresses encountered in the W/ZrO$_2$ during the shutdown transient are much less severe than the startup transient stresses.

Reducing the chamber pressure to 300 psia would not solve a transient stress problem in the W/ZrO$_2$ barrier for the low temperature ($\bar{T}$ < 1500°F) elastic stress range unless provision for a ramped start were also made.

VI, E, Thermal Analysis (cont.)

> A relatively long duration (1.0 sec or greater) start ramp is required to affect significant reductions in the transient stresses.
>
> Stress reductions obtained with a stepped ramp which provides for holds at intermediate P_c levels may be duplicated by a simple linear P_c ramp; therefore, a complicated programmed system startup is not required.

3. Chamber Temperature Transients

The temperature response at five locations in the coating and nickel channel at the chamber throat for a stepped (step function) combustor start are shown in Figure 35. The temperature rise curves after engine ignition (FS-1) and the temperature decay curves following shutdown (FS-2) are typical of the predicted wall temperature obtained with the thermal model for the various engine cycles investigated. Referring to Figure 35, it is seen that a stepped combustor startup produces a rapid increase in tungsten liner temperature after FS-1. The tungsten temperature is seen to approach steady state in approximately 2 sec. The inner nickel shell temperature (T_3 and T_4) lags the tungsten temperature and does not reach equilibrium until approximately 3 sec after FS-1. This temperature lag is attributed to the thermal capacitance and very high thermal resistance of the W/ZrO_2 thermal barrier which impedes the flow of heat from the tungsten liner to the outer nickel shell. For the same reason, the outer nickel shell temperature lags the inner shell and requires approximately 4 sec to reach steady state. At this time, the chamber wall at the throat will be at thermal equilibrium.

The channel and coating temperature decay curves which occur after combustor shutdown (FS-2) are nearly the reverse of the startup curves except that the slope of the decay curves are much reduced compared to the startup curves. The outer shell temperature is also seen to lag the tungsten temperature by nearly 0.5 sec. This very long temperature lag is primarily attributed to the thermal capacity of the nickel channel which is relatively high compared to the coating and tends to maintain the channel temperature constant while the coating temperature decreases. Another factor that contributes to the channel temperature lag is that the film coefficient of the hydrogen coolant is relatively low at the beginning of the transient because of the high channel wall temperatures. The lower film coefficient reduces the heat flux into the coolant.

4. Combustor Ramping Effects

A ramped combustor startup or shutdown reduces the slope of the wall temperature-time curves and also promotes heat soakback through the coating into the nickel channel. These effects tend to reduce the temperature

VI, E, Thermal Analysis (cont.)

gradients in the coating and in the channel. Since a reduction of temperature gradient also reduces thermal shock and hoop stresses during the thermal transient, a ramped combustor startup or shutdown should be employed to reduce the coating and channel stresses during the startup and shutdown thermal transients.

F. STRESS ANALYSIS

1. Configuration

Aerojet Drawings 1146502, Mandrel, Coated Combustion Chamber, and 1146503, Combustion Chamber Channel Detail, establish the basic dimensions and configurations. Figure 1 is a representation of these drawings. Figure 32 depicts the finite element layout of a symmetrical section at the throat and is the area to be analyzed in this study.

2. Pressure and Thermal Conditions

The chamber pressure was 400 psi and the coolant channel pressure at the throat was 730 psi.

The temperature data used in this study were for a step function start, 2-sec ramp start, and a step function shutdown and are given in Tables V through VII. The thermal distribution across the throat section at steady state is given in Reference 1. The temperature profile locations are indicated below:
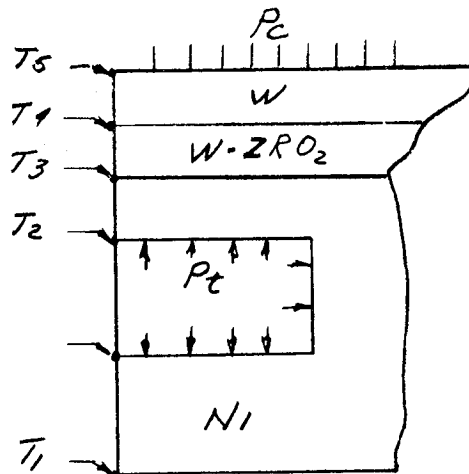
3. Material Properties

The material properties used in the analysis were obtained from Reference 1.

VI, F, Stress Analysis (cont.)

4. Detailed Finite Element Analysis of Shutdown

Since there was concern that the chamber at steady state temperatures (maximum average temperature conditions) with no chamber pressure ($P_c = 0$) could not contain the thermal loads plus the coolant pressure loads, the step function shutdown analysis was made first. The results which are summarized in Table VIII did not significantly vary from the steady-state analysis. The maximum compressive hoop strain in the tungsten increased from 1.2% to 1.32%. The maximum hoop tensile stress in the nickel decreased from 53,100 to 40,100 psi. The margin of safety of the nickel:

$$MS_{Yield} = \frac{85,000}{40,100} - 1 = +1.1$$

5. Startup and Shutdown Transient Analyses

The results of the approximate finite element analyses for the step function start, two second ramp start, and step function shutdown are shown in Figures 36 through 38. The stresses shown represent the gross stresses at the locations indicated and do not account for local stress variations. However, the results do give a comparative indication of the effects of the thermal transients as follows:

- The step function start and two second ramp start do not produce adverse stresses in the throat section compared to the steady-state values.

- The step function start and ramp start produce higher compressive stresses in the tungsten materials and higher tensile stresses in the electroformed nickel than during steady state as indicated on Figures 36 and 37. The only difference between the two starts is that the maximum stress is developed at different times.

Step Start

$$Ni: \quad MS_{Ult} = \frac{110}{57.8} - 1 = +0.90$$

Two Second Ramp

$$Ni: \quad MS_{Ult} = \frac{110}{60.2} - 1 = +0.82$$

VI, F, Stress Analysis (cont.)

The stresses developed at the throat after cooldown with
730 psi in the channels and prior to firing are as follows:

W: σ_{Hoop} = -42,310 psi

W/Zr: σ_{Hoop} = -14,980 psi

Ni: ID

σ_{Hoop} = 20,350 psi

OD

σ_{Hoop} = 18,950 psi

The step function shutdown increases the maximum compressive
stress in the tungsten materials and increases the maximum tensile stress in
the nickel compared to steady state. All stresses are well within allowables:

Ni: σ_{Hoop} = 51,400 psi

$$MS_{\text{Ult}} = \frac{110}{51.4} - 1 = +1.1$$

G. OTHER CONSIDERATIONS

The thermal analyses assumed fully established liquid hydrogen
coolant flow in the coolant channels and did not consider the problem of
establishing the flow. Since the cooling circuit hydrogen is supplied
separately from the injector hydrogen flow, the coolant flow may be estab-
lished by providing for sufficient coolant lead time prior to FS-1. This
coolant lead will be a period of chamber cooldown. The time required for
coolant lead would best be determined by cold flowing the chamber cooling
system without firing the chamber. This might be accomplished during the
scheduled cold flow thermal shock testing by using coolant outlet pressure
and temperature instrumentation to calculate the required lead time.

An injector fuel lead startup is recommended since an oxidizer
lead would produce stoichiometric mixtures and very high gas temperatures
($\sim$9000°R) sometime during the transient. A fuel-rich startup circumvents
the potential thermal problems which could occur during an oxidizer-rich
startup. For the same reason, on shutdown the injector oxidizer valves
should be closed prior to closing the fuel valve. A fuel-rich startup and
shutdown are also consistent with the cooling requirements for the Rigimesh
face cooled injector that will be employed for the testing. Also, the

VI, G, Other Considerations (cont.)

thermochemical analysis performed during the design phase of the program (Reference 1) indicates corrosion of the tungsten liner could result from an oxidizer-rich propellant mixture.

Thermal shocking the plating should not be a problem during the shutdown transient provided normal injector and chamber purge procedures are employed. A low volume GN_2 gas purge flow at ambient temperature will suffice to purge the system. A long injector hydrogen flow transient which could permit liquid H_2 injector flow should be avoided since this could thermal shock the tungsten liner. A recommended startup and shutdown procedure (after passivation) is delineated below.

H. RECOMMENDED STARTUP AND SHUTDOWN PROCEDURE

Although the stress analysis performed indicates that a step function start and step function shutdown are acceptable, prudence requires that, if the equipment capability exists, a 2- or 3-sec ramp start should be adopted. A step function shutdown is recommended, incorporating the fuel-rich shutdown and purge procedure outlined below.

Startup

1. LF_2 and LH_2 lines and injector circuit cooled to -200°F minimum.

2. Obtain full H_2 flow in coolant circuit before startup.

3. Fuel and oxidizer prefire purge "ON". Purge pressure to be regulated to obtain at least 20 psig in manifolds. Purges to be check-valved off or turned off 2 to 3 sec before TCV openings.

4. Fuel TCV opening to lead oxidizer TCV opening by 0.075 ± 0.025 sec.

5. Fuel and oxidizer valve rate of opening to be the same.

Shutdown

1. Fuel TCV closing to follow oxidizer TCV by 0.075 ± 0.025 sec.

2. Postfire oxidizer purge "ON" at FS-2. Purge pressure ∿150 psig. Purge duration 5 sec minimum.

VI, H, Recommended Startup and Shutdown Procedure (cont.)

3.   Postfire fuel purge "ON" at fuel TCV closing signal. Purge pressure ∿150 psig. Purge duration 5 sec minimum.

4.   Fuel and oxidizer TCV rate of closing to be the same.

5.   Signal coolant circuit valve closed at same time as fuel TCV. Closing rate ∿0.2 to 0.3 sec. Obtain partial flow ∿20% by a bypass system around main valve or by leaving valve partially open. Flow 1 to 2 sec.

6.   Introduce GHe coolant circuit purge upon closing of coolant circuit valve. Purge pressure 150 psig minimum. Purge duration 5.0 sec minimum.

VII. CONCLUSIONS AND RECOMMENDATIONS

Review of the fabrication experience and the results obtained point to the conclusion that the basic concept followed in the design and fabrication of the thrust chamber is feasible; however, both the vapor deposition process and the electroforming process require additional study and development. Also, additional process steps and controls should be incorproated in the general procedure to ensure that dimensional tolerances and quality levels are maintained.

Specific areas in the vapor deposition of tungsten that require further development are:

(1) Application of the tungsten screen to the graphite mandrel without butt or lap joints and voids or gaps between the screen and mandrel. The applicability of three-dimensional contour weaving should be investigated.

(2) Heat source for the graphite mandrel with controls capable of obtaining uniform temperatures throughout the substrate.

The use of electroforming for obtaining structures requires:

(1) Specifications and standards to establish physical and mechanical properties and, further, the development of process controls and nondestructive test methods to ensure that the required properties are obtained.

(2) Further study to determine the relative merits and limits of "growing" the ribs as was done in this program versus machining the ribs.

Process steps that should be added to the fabrication procedure are:

(1) Contour grinding of plasma-arc-sprayed coatings to ensure dimensional control.

(2) Inspection of conductive coatings applied to nonconductive substrates for complete homogeneity and integrity.

(3) Flow testing of coolant channels immediately after removal of core material to ensure even flow distribution and that the core material is entirely removed.

NOMENCLATURE

D_e = Equivalent diameter

C_L = Coolant heat transfer coefficient factor for curvature

h_L = Coolant heat transfer coefficient

k = Thermal conductivity

P_c = Chamber pressure

Pr = Prandtl number

T = Temperature

V = Velocity

μ = Dynamic viscosity

ν = Kinematic viscosity

ρ = Density

σ = Stress

Subscripts

b = Bulk coolant

f = Film

r = Recovery

w = Wall

o = Sink (ambient)

∞ = Free stream

REFERENCES

1. Stubbs, V. R., Evensen, H. M., Fraczek, E. W., Cunningham, J. A., "Interim Report Covering Task I, Investigation of Advanced Regenerative Thrust Chamber Designs," NASA CR-72266, Contract NAS 3-7971, August 1967.

2. Budzenski, J. A., "Heat Transfer (Noncryogenic and Cryogenic)," Aerojet Computing Sciences Program E25106, 11 August 1969.

3. "Design Equation Analysis for Heat Transfer to Cryogenic Hydrogen at Pressures from 600 to 1500 psia and Wall-to-Bulk Temperature Ratio to 20," Aerojet NERVA Program, Contract SNP-1, Report No. RN-S-0274, June 1966.

TABLE I

CHEMICAL VAPOR DEPOSITION OF TUNGSTEN
SUMMARY OF EXPERIMENTAL RUNS

Experiment No.	Objectives	Results	Remedial Action
1	Equipment and process checkout	Leaking helium pressure regulator permitted over-pressure to 8 psi during leak test operation. Quartz window broke under overpressure.	1. Installed safety relief valve. 2. Replaced quartz window. 3. Replaced helium pressure regulator.
2	Equipment and process checkout	Max temperature obtainable in graphite was 288°F after 16 hr.	1. 750-watt lamp replaced with 1000-watt lamps. 2. Inside of chamber lined with aluminum foil for maximum reflectivity.
3	Equipment and process checkout	Max temperature after 14 hr was 525°F. The rotating mechanism, seals and gaskets performed well.	1. Outside of chamber wrapped with aluminum-backed fiber-glass insulation. 2. Three 1000-watt lamps added to heater. 3. Bottom of chamber insulated with Fiberfrax woven insulation. 4. Coolant water system repiped to permit the water to the walls and top of the chamber to be shut off and still cool the window, lamps, and reactive gas manifold.
4	Equipment and process checkout	Exhaust system plugged after 20 min of operation; window gasket began to leak.	1. Liquid trap installed in the exhaust system. 2. A dual exhaust system was installed. 3. Vistanex was substituted for RTV 60 as the gasket sealant.

TABLE I (cont.)

Experiment No.	Objectives	Results	Remedial Action
5	Equipment and process checkout	After 25.5 hr, a temperature of 665°F was reached. A fuse failure shut power off for 2 hr. After resumption of heating for 20 min, the rotating mechanism malfunctioned.	1. Clearance increased between packing unit, lower seal housing, and rotating shaft for increased clearance to allow for differences in thermal expansion.
6	Equipment and process checkout	Quartz window fogged up, preventing the infrared radiation from entering the chamber.	1. Quartz glass window reground and polished. 2. Entire reactive gas piping system dismantled and cleaned piece by piece, then sealed from the atmosphere. 3. Gas cooling manifold installed to cool outside of quartz window with nitrogen.
7	Equipment and process checkout	After plating for 3.5 hr, the quartz window temperature increased and the mandrel temperature decreased, forcing shutdown.	1. Investigated induction heating to replace infrared lamp unit. 2. 23 KW induction unit installed and pancake induction coil designed.
8	Induction coil checkout in air.	Satisfactory heating rate established; spark gap checked out.	
9	Calibration test of induction coil with screen on mandrel.	Screen edges glowed red when passing under the coil. After 6 hr of operation, the test was discontinued at 525°F mandrel temperature because coil arced to screen.	1. Screen fitted tighter to mandrel.

TABLE I (cont.)

Report NASA CR-72742

Experiment No.	Objectives	Results	Remedial Action
10	Calibration test of induction coil with screen on mandrel	Screen edges glowed red when passing under coil.	1. Devised better retention method for screen.
11	Calibration of induction coil and test cooling system for induction coil and gas manifolds.	Epoxy joints in mandrel outgassed. Screen turned blue wherever contact with graphite was not good. The inlet water for the reactive manifolds was at 90°F, but flow was low and exit water was at 160°F.	1. Eliminated epoxy for bonding and pinned the parts together. 2. Added recirculating cooling system for induction coil and gas manifolds. 3. Flame sprayed mandrel with 18-8 SS and a flash of copper, then spot welded the screen to the coating.
12	Evaluate heating of the spot welded screen and effectiveness of the recirculating system.	Recirculating cooling system performed satisfactorily. At near 400°F, screen developed brown spots, indicating that it was overheating. When power was turned up, screen glowed red.	1. Prepared a graphite mandrel for Cal-Rod heating.
13 and 14	Calibration tests using Cal-Rod heating	Cal-Rods performed satisfactorily.	
15	Establish plating rates versus tempera-	Electric short occurred, causing water leak into chamber. A restriction in the exhaust system forced shutdown after 11 hr. Plating thickness varied from 0.0034 to 0.0064 in.	1. A grounding strap was applied to the rotating shaft. 2. Examined photomicrographs of coating and determined deposition rate. Temperature at each zone was corrected to increase or decrease deposition rate, as applicable. 3. Designed and installed new exhaust system.

TABLE II

WATER FLOW TESTS

Test No.	Inlet Pressure, psig	Back Pressure, psig	Pressure Drop, psig	Flow Rate, lb/sec	ΔH Daniels Plate	Ratio $\Delta H/\Delta P$	Avg of Ratios	K_w	Pressure Drop, psi @ 15 lb/sec flow
Inlet to Outlet									
1a	372.0	Atmos	372.0	14.08	100.0	0.2688			
1b	408.0		408.0	14.76	110.0	0.2696	0.2693	0.7305	421.5
1c	445.0		445.0	15.42	120.0	0.2696			
Manifold to Manifold									
2a	--	204.0	353.0	14.07	100.0	0.283			
2b	--	200.0	391.0	14.77	110.0	0.281	0.282	0.7470	403.2
2c	--	206.0	400.0	14.95	113.0	0.282			
Inlet to Outlet									
3a	528.0	158.0	370.0	14.36	104.0	0.281			
3b	553.0	168.0	385.0	14.73	109.5	0.284	0.289	0.756	393.6
3c	552.0	175.0	377.0	15.05	114.5	0.303			
Inlet to Outlet									
4a	400	8	392	14.73	109.5	0.279	0.279	0.743	407.2

TABLE III

OPERATING CONDITIONS ANALYZED

	Nominal	Off-Design		
Chamber pressure, psia	400	400	400	300
Mixture ratio, O/F	12	12	12	8
Hydrogen coolant inlet temperature, °R	60	60	60	60
Hydrogen coolant outlet pressure, psia	550	550	550	400
Coolant flow rate, % of fuel flow through injector	100	125	150	100
Total injector flow rate, lb/sec	18.4	18.4	18.4	13.8
Coolant flow rate, lb/sec	1.42	1.77	2.12	1.53
Combustion product stagnation temperature, °R	7654	7654	7654	6657

TABLE IV. — SUMMARY OF RESULTS

	Nominal		125% Coolant Flow	150% Coolant Flow	P_c=300 MR=8.0
	Ref 1	Present 1-D			
Coolant inlet pressure, psia	760*	760	821	884	647
Coolant outlet temperature, °R	490**	490	406	351	367
Maximum chamber conditions:					
Coating temperature, °F	4460	4590	4500	4450	3460
Nickel temperature, °F	1300	1520	1320	1210	1060
Coolant surface temperature, °F	1000	1170	1000	870	800
Heat flux, Btu/in.^{2}-sec	7.4	7.4	7.6	7.7	5.7
Throat conditions:					
Coating temperature, °F	4250	4250	4200	4150	3140
Nickel temperature, °F	780	920	790	690	530
Coolant surface temperature, °F	410	540	410	320	280
Heat flux, Btu/in.^{2}-sec	8.2	7.9	8.0	8.1	6.2
Gas-side heat transfer coefficient, Btu/in.^{2}-sec-°F	0.00262	0.00260	0.00261	0.00261	0.00198
Coolant heat transfer coefficient, Btu/in.^{2}-sec-°F	0.0118	0.0096	0.0112	0.0127	0.0103

---

*Coolant outlet pressure was 547 psia in Reference 1 vs 550 psia herein.
**Coolant inlet temperature was 50°R in Reference 1 vs 60°R herein.

TABLE V. – TEMPERATURE DATA, THROAT REGION–STEP FUNCTION START

Temperature Profile

Time (sec)	T_1 (°F)	T_2 (°F)	T_3 (°F)	T_4 (°F)	T_5 (°F)
0.2	−390	−280	−270	1000	1100
0.3	−360	−180	−120	1750	1960
0.4	−320	−40	40	2400	2620
0.5	−270	80	220	2840	3040
0.6	−215	200	390	3140	3340
0.8	−160	420	660	3520	3700
1.0	−100	600	870	3740	3920
1.2	−60	740	1010	3880	4050
1.4	−40	840	1110	3970	4140
1.6	−20	910	1170	4040	4200
1.8	0	960	1220	4070	4240
2.0	20	995	1250	4100	4260

TABLE VI.- TEMPERATURE DATA, THROAT REGION-TWO SECOND RAMP START

Temperature Profile

Time (sec)	T_1 (°F)	T_2 (°F)	T_3 (°F)	T_4 (°F)	T_5 (°F)
0.2	-395	-370	-339	117	139
0.4	-374	-335	-287	422	465
0.6	-344	-284	-212	845	912
0.8	-301	-215	-118	1309	1401
1.0	-249	-141	-7	1772	1884
1.2	-196	-82	145	2212	2343
1.4	-155	-29	296	2621	2769
1.6	-116	60	443	2991	3151
1.8	-83	144	600	3322	3491
2.0	-53	209	749	3616	3792
2.2	-25	267	872	3806	3977

TABLE VII - TEMPERATURE DATA, THROAT REGION-STEP FUNCTION SHUTDOWN

Temperature Profile

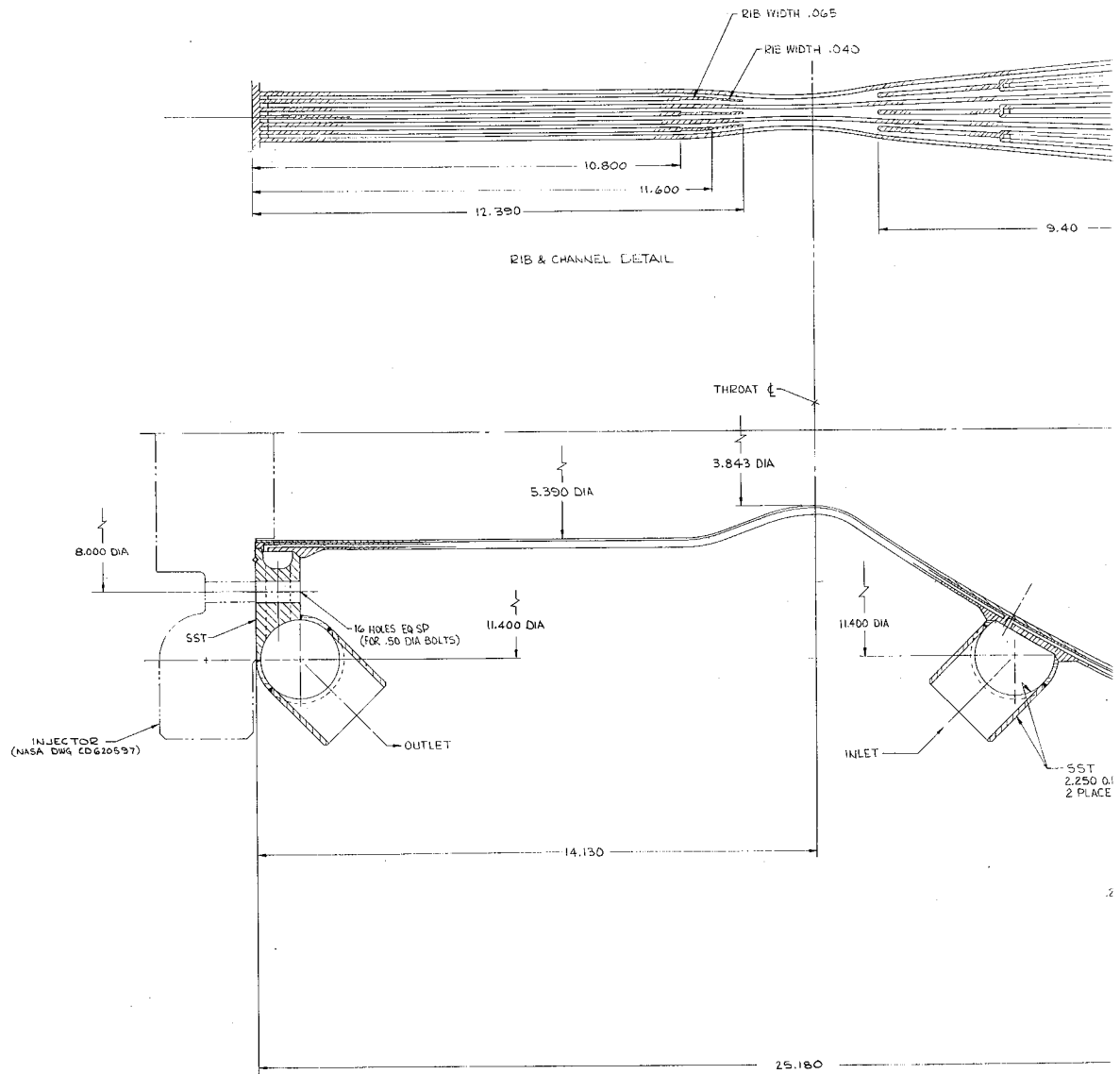| Time (sec)	T_1 (°F)	T_2 (°F)	T_3 (°F)	T_4 (°F)	T_5 (°F)
0	110	1100	1350	4180	4340
0.2	110	1070	1310	3800	3900
0.4	110	940	1160	2900	2940
0.6	90	720	910	2200	2220
0.8	40	500	660	1640	1660
1.0	-20	300	410	1200	1220
1.2	-80	120	200	860	880
1.4	-140	-30	20	560	570
1.8	-280	-240	-220	120	130
2.0	-340	-300	-280	-50	-40

TABLE VIII - DETAILED FINITE ELEMENT ANALYSIS RESULTS*

THROAT SECTION

SHUTDOWN

$$P_c = 0$$
$$P_t = 730 \text{ psi}$$

Material	Thickness (inches)	Location Radii (inches)	Hoop Stress (psi)	Effective Stress (psi)	Condition	Percentage Strain	Temp °F
Tungsten (W)	0.030	1.90 - 1.93	-10,290	10,180	Plastic	1.32	4036
88% w - 12% ZrO$_2$	0.016	1.93 - 1.946	-20,670	20,670	Plastic	0.96	2788
75% w - 25% ZrO$_2$	0.009	1.946 - 1.955	-25,700	25,900	Plastic	0.81	1931
50% w - 50% ZrO$_2$	0.012	1.955 - 1.967	-33,800	34,080	Plastic	0.46	840
Ni-Alloy	0.002	1.967 - 1.969	-35,460	34,600	Plastic/Elastic	0.42	806
Ni	0.030	1.969 - 1.999	-44,730	43,720	Plastic/Elastic	1.25	555
Ni	0.060	1.999 - 2.059	+41,000	40,000	Elastic	0.14	-61

RIB WIDTH .065

RIB WIDTH .040

10.800

11.600

12.390

9.40

RIB & CHANNEL DETAIL

THROAT ℄

3.843 DIA

5.390 DIA

8.000 DIA

16 HOLES EQ SP
(FOR .50 DIA BOLTS)

11.400 DIA

11.400 DIA

SST

INJECTOR
(NASA DWG CD620537)

OUTLET

INLET

SST
2.250 O.
2 PLACE

14.130

25.180

W .030 THICK
88W-12 ZrO₂ .016 THICK
75W-25 ZrO₂ .009 THICK
50W-50 ZrO₂
(A) .012 THICK FROM FORWARD END
TO THROAT.
(B) THICKNESS VARIES UNIFORMLY
FROM .012 THICK AT THROAT
TO .044 THICK AT INLET.
(C) .044 THICK FROM INLET TO AFT END.
PLASMA ARC SPRAYED NICKEL .003 THICK
ELECTRO DEPOSITED NICKEL
CHANNEL HEIGHTS:
(A) .080 FROM FORWARD END TO CYLINDRICAL
TO CONICAL TRANSITION OF CHAMBER.
(B) CONSTANT TAPER HEIGHT FROM .080 TO .060
FROM CYLINDRICAL/CONICAL TRANSITION OF
CHAMBER TO THROAT.
(C) CONSTANT TAPER HEIGHT FROM .060 TO .100
FROM THROAT TO AFT END.

.030
.060
.090

COATING & CHANNEL DETAIL
SCALE NONE

2°30' 48 PLACES
7°30' 48 PLACES
2°30' 48 PLACES
3°45' 48 PLACES

.050 THK ZrO₂
15.272 DIA
15.850 DIA
9 WALL
19.388 DIA
S ST
A BOLTS
ACES
PACED

CARBON PHENOLIC WB 8217 (TAPER FROM .650 AT FWD END
TO .450 AT EXIT)
WRAP ORIENTATION
PARALLEL TO ₵
GLASS CLOTH
& ROVING
SILICA-PHENOLIC
(FLAT WRAP)
WB 2230
(.350 THICK)

29.768 DIA

27.840

Figure 1. Regeneratively Cooled Thrust Chamber Assembly

43
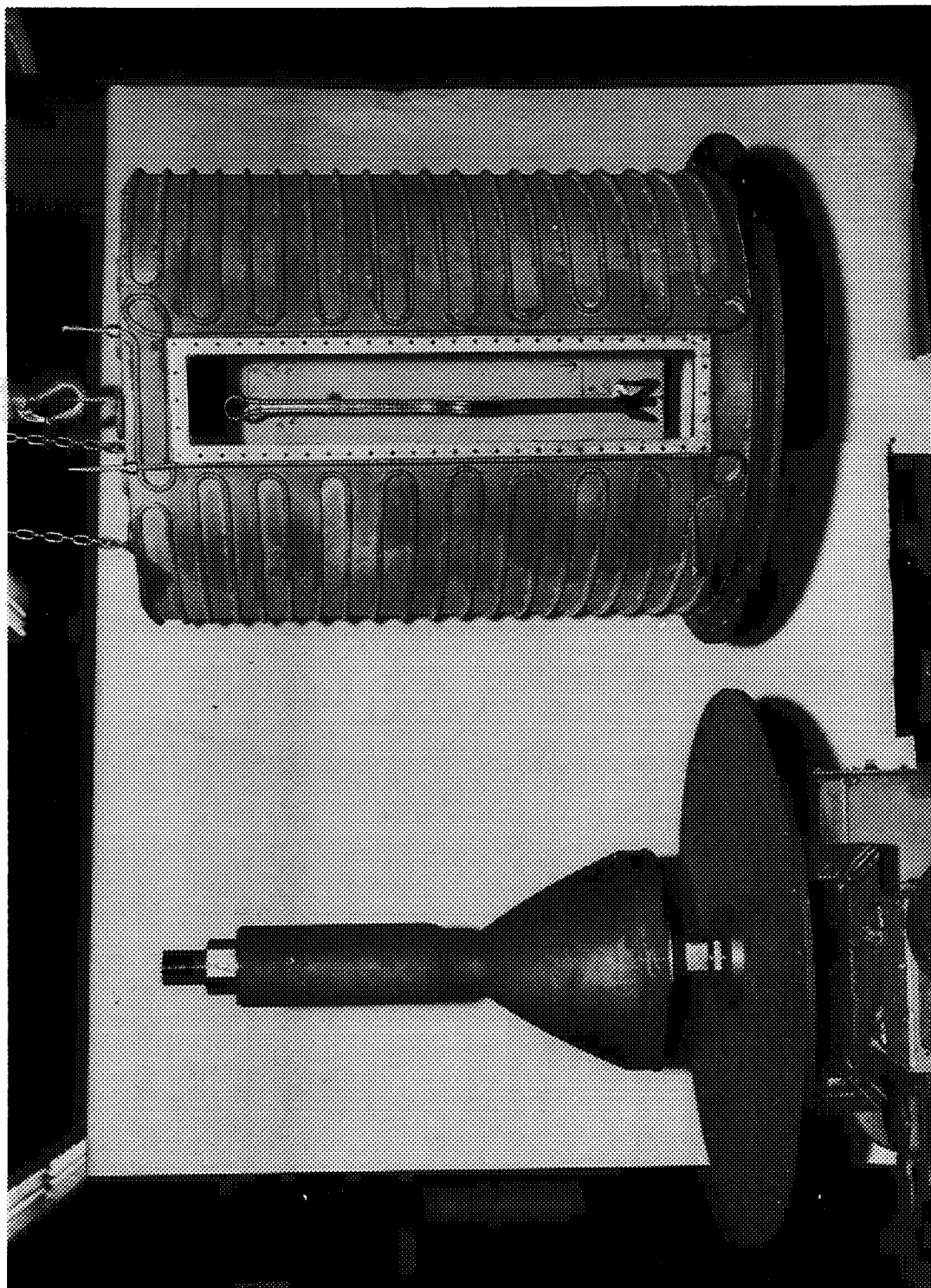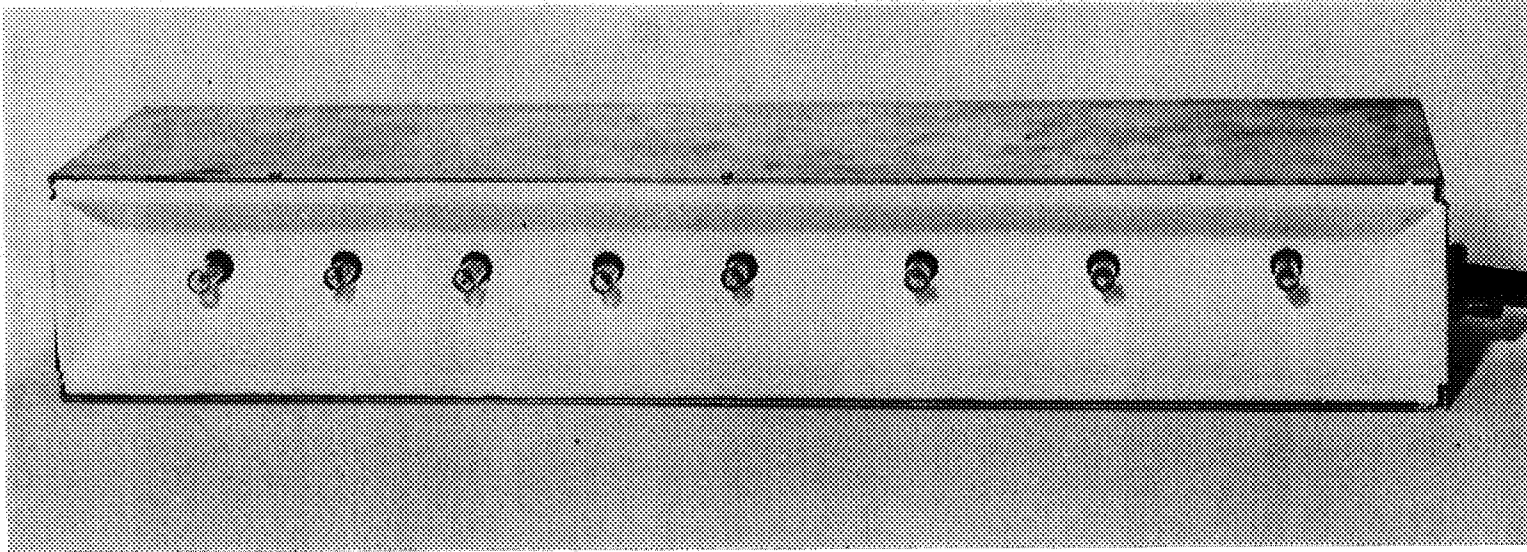
Figure 3.   Infrared Quartz Lamp Assembly Before Modification

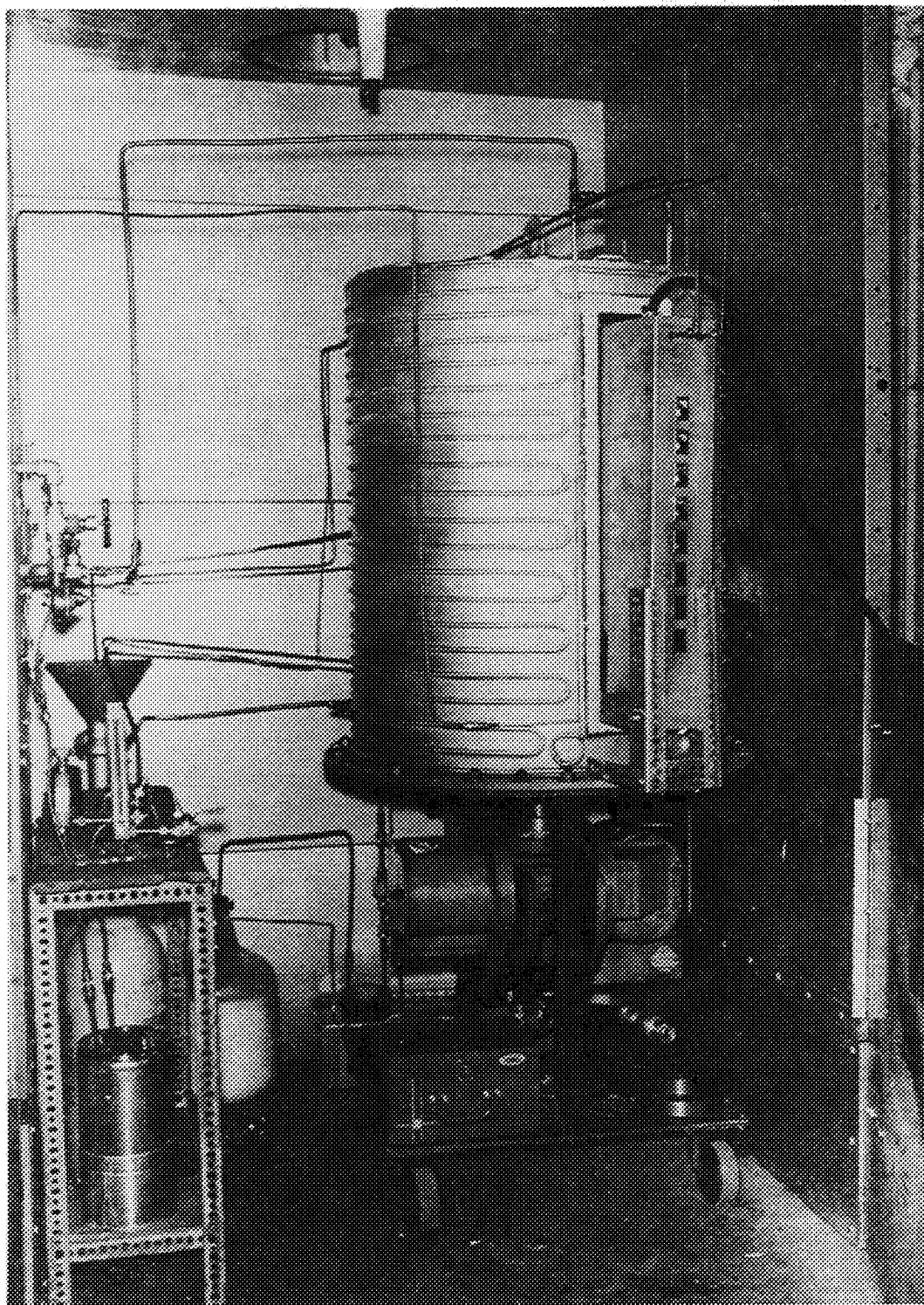Figure 4. Deposition Chamber Under Sparkproof Hood with Infrared
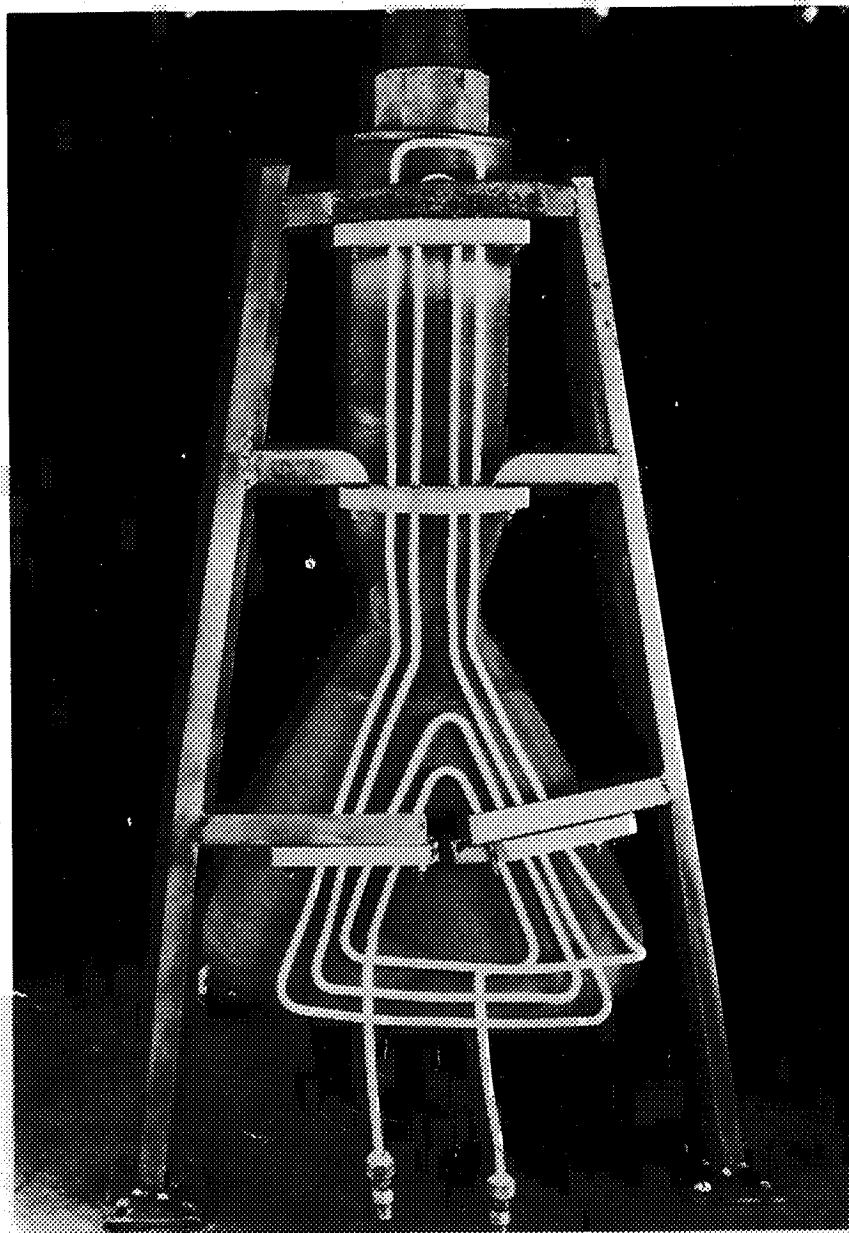Lamps Assembled to Quartz Window

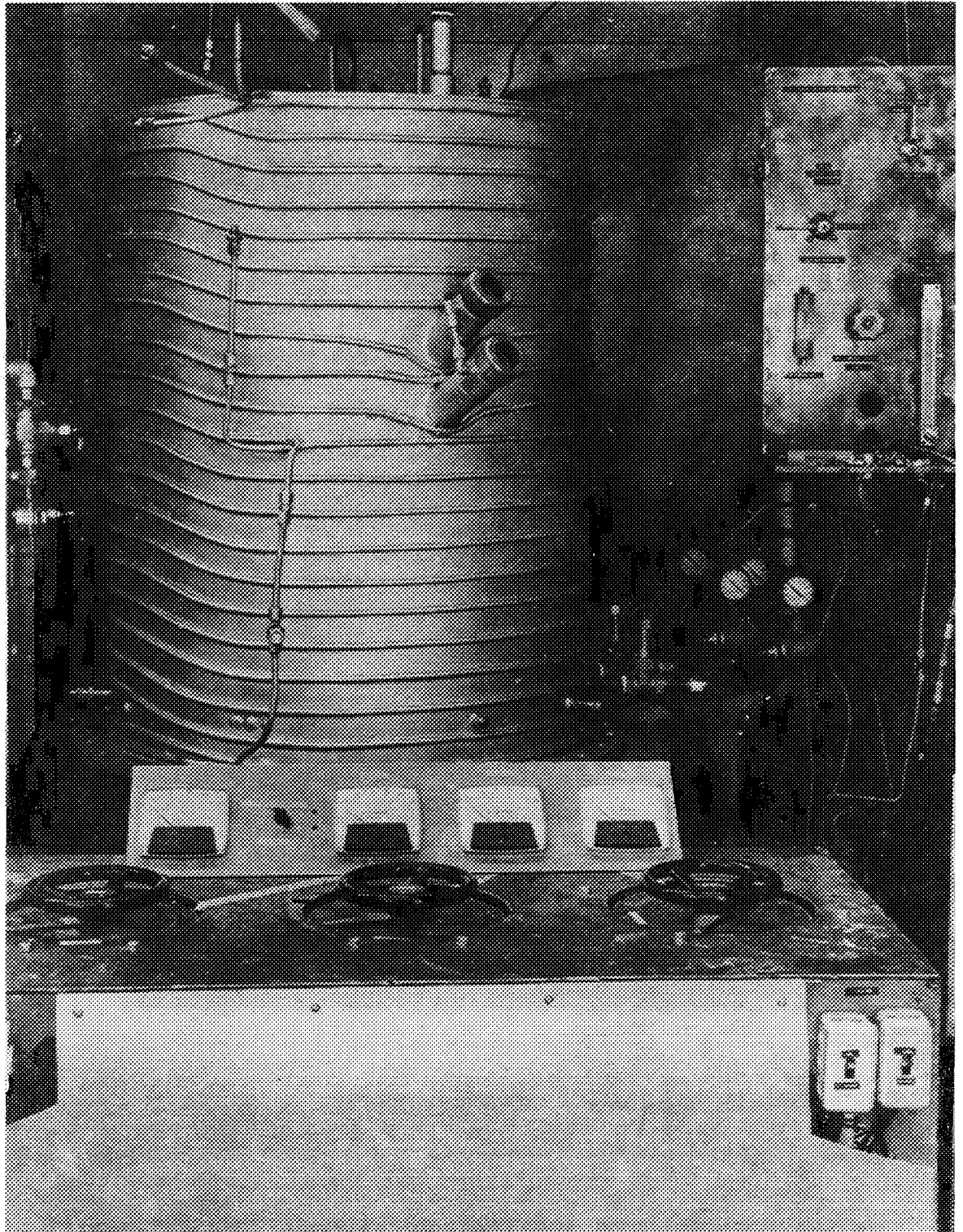Figure 5. Al_2O_3 Coated Induction Coil with Test Graphite Mandrel

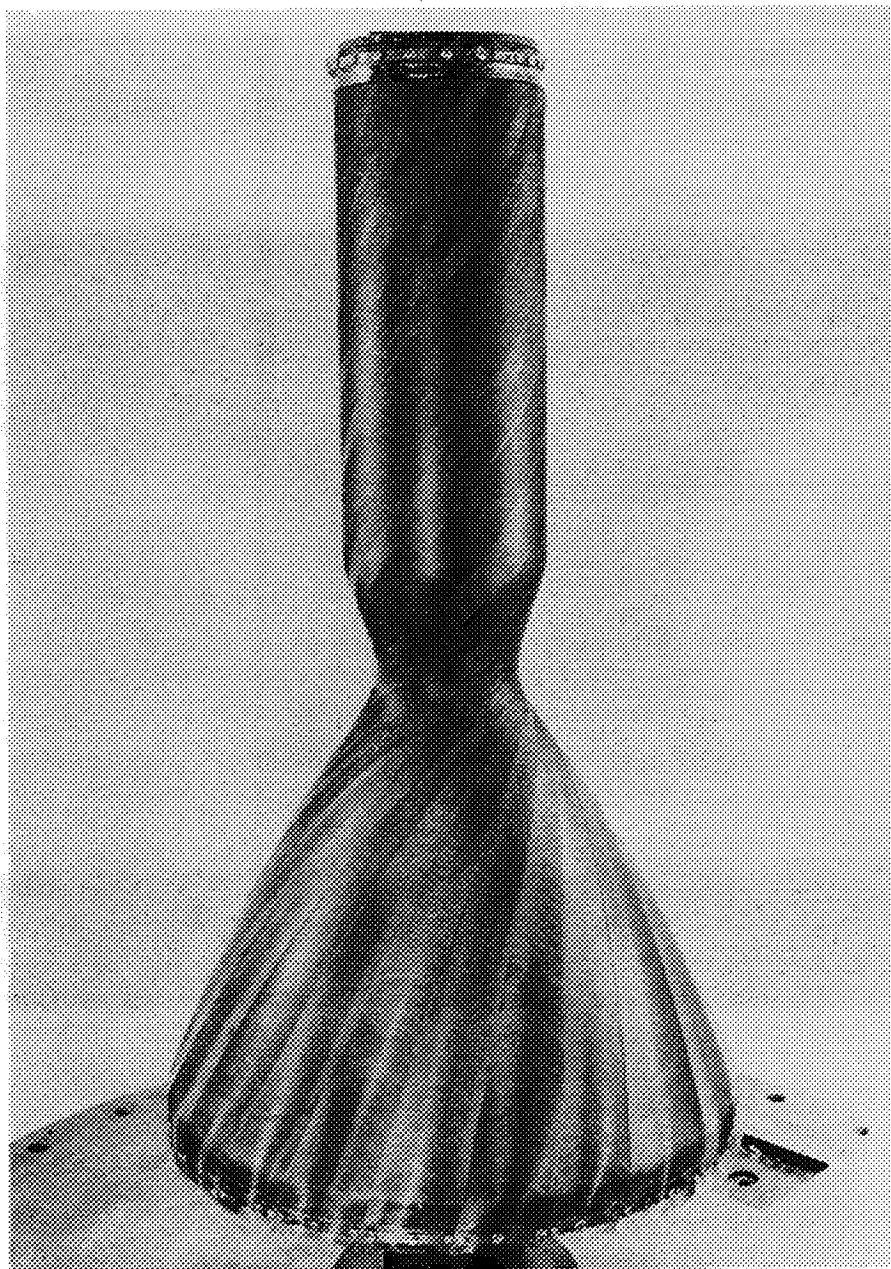Figure 6. Vapor Deposition Equipment Showing Cal-Rod Control Variac

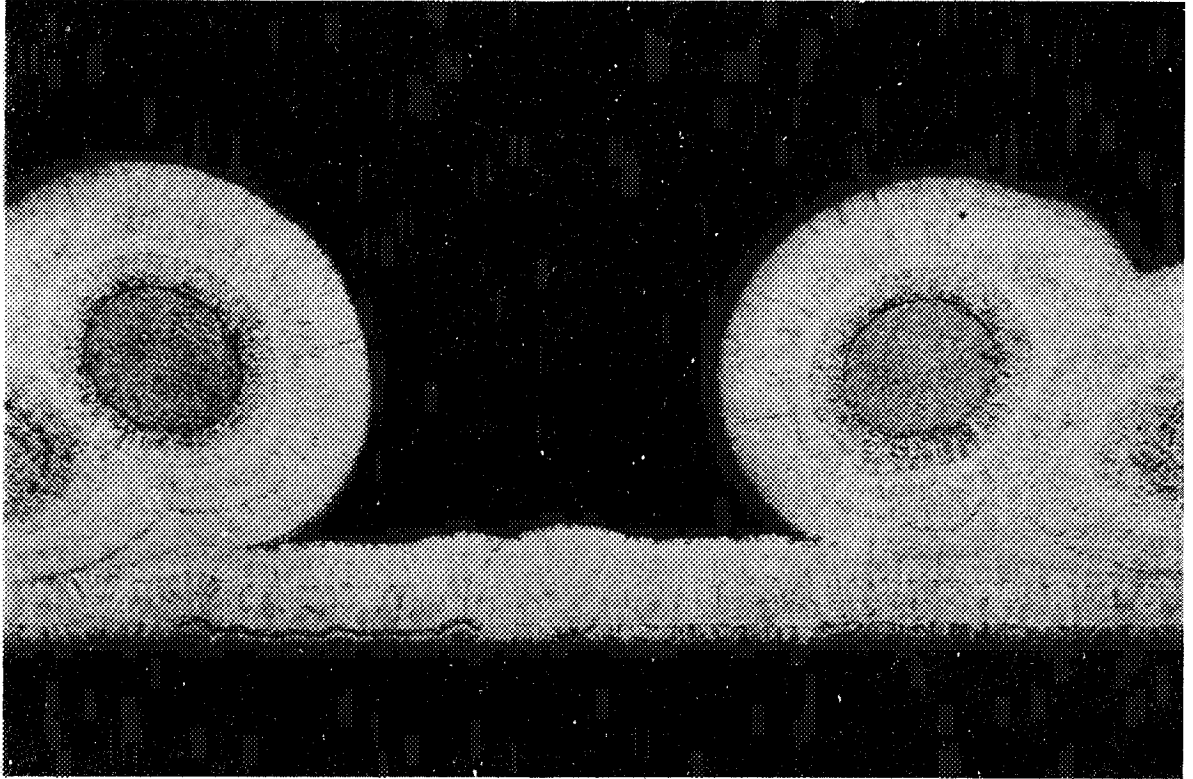Figure 7. Mandrel with Tungsten Screen Assembled

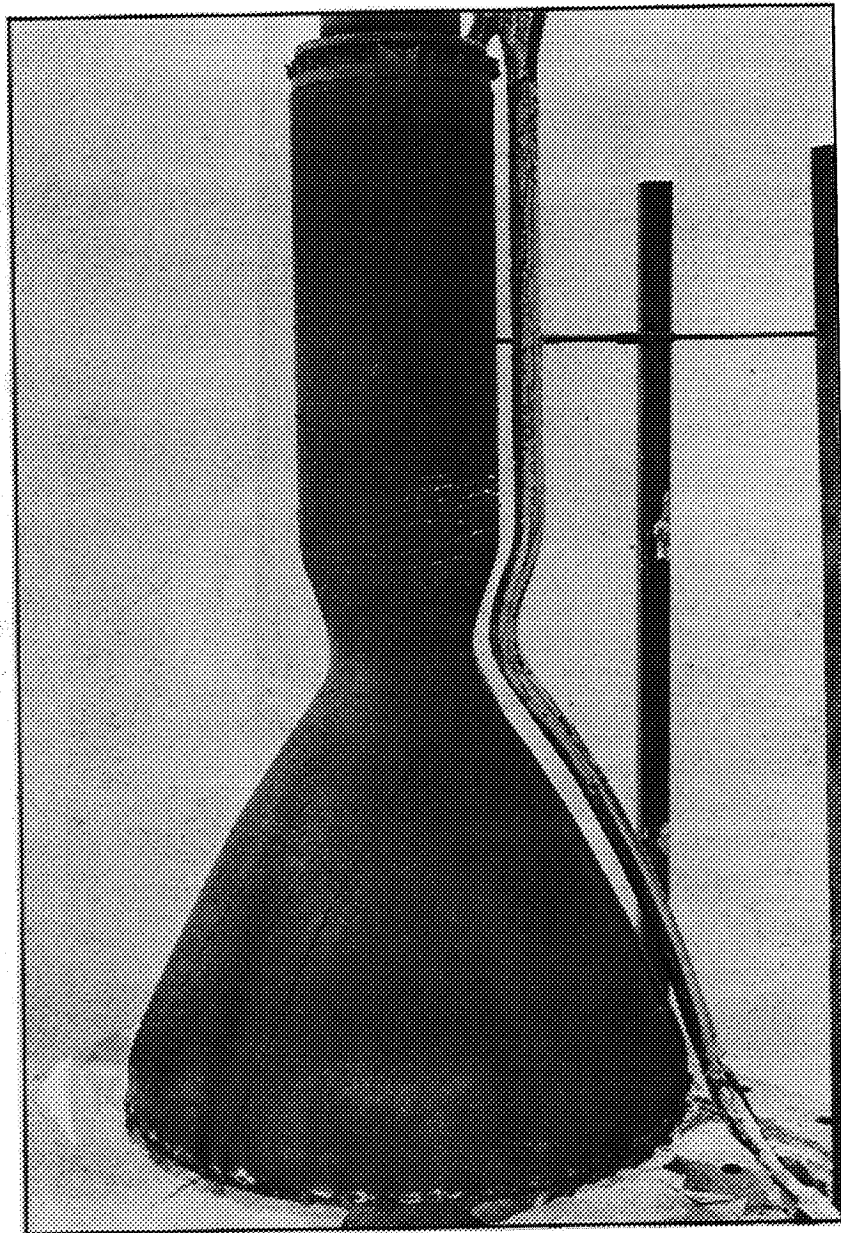Figure 8.   Specimen of Screen from Test Run 15 - 100X

Figure 9. Vapor Deposited Tungsten, Wire Mesh Reinforced Thrust
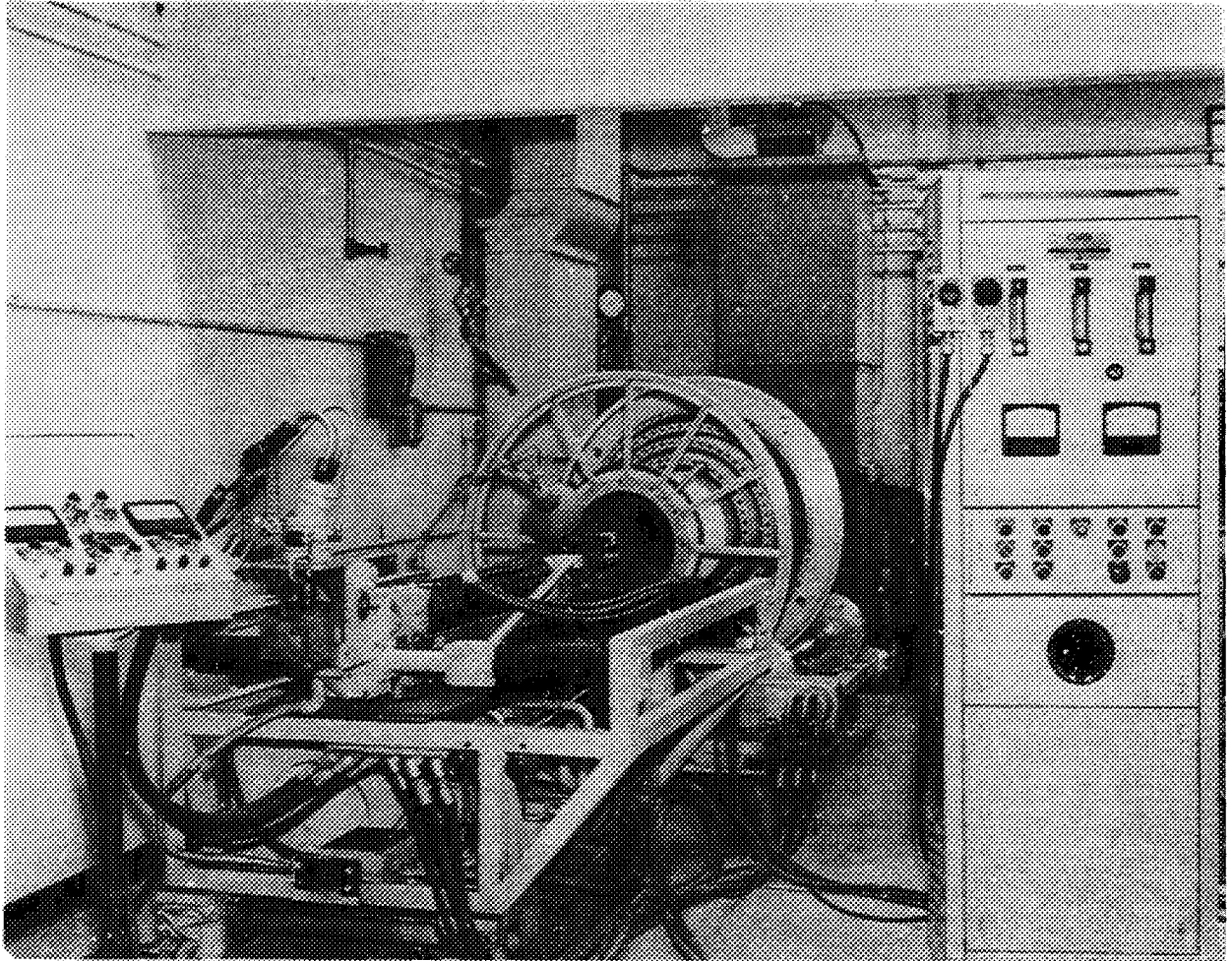Chamber Flame Liner, as Deposited on Graphite Mandrel

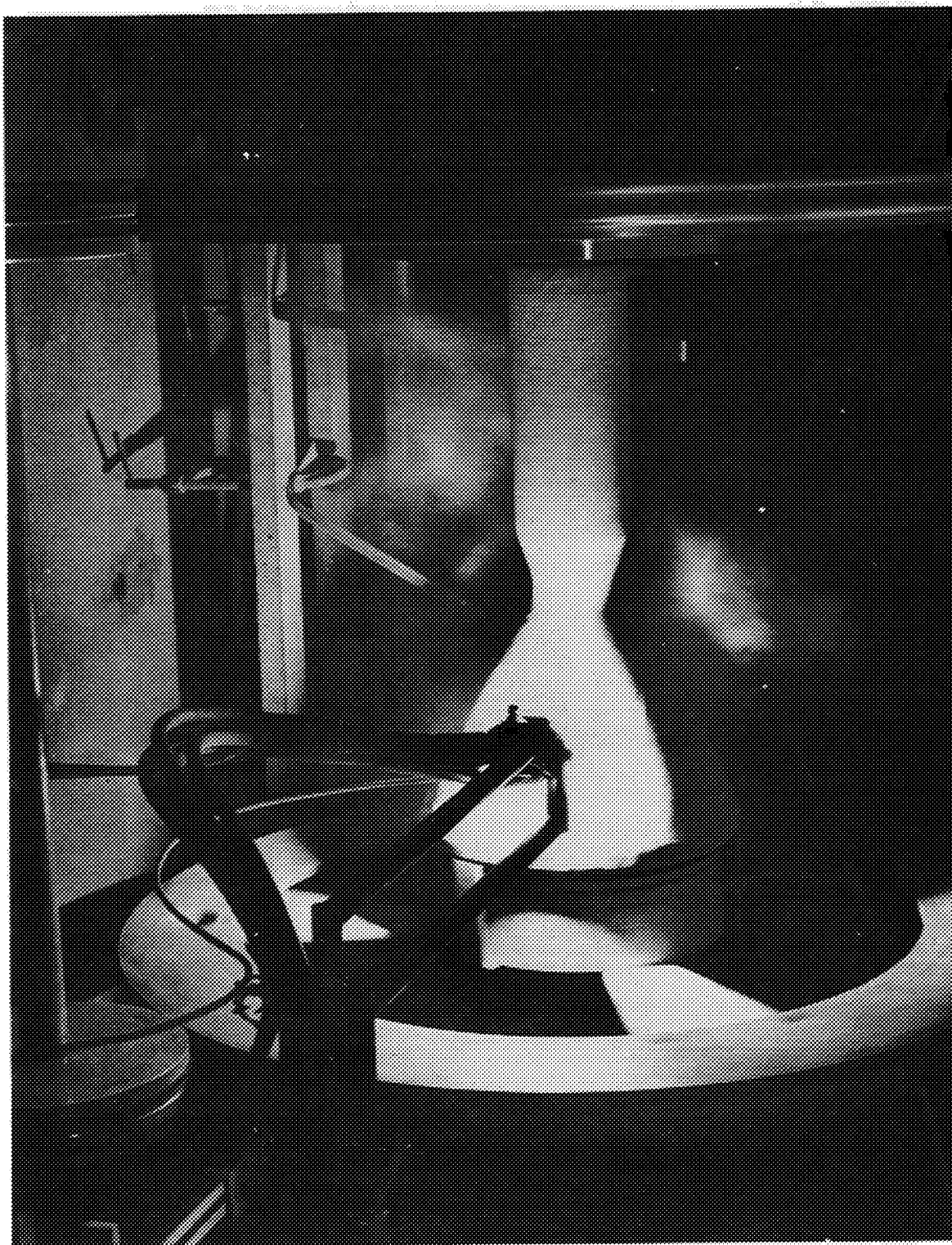Figure 10. Plasma Arc Facility and Equipment
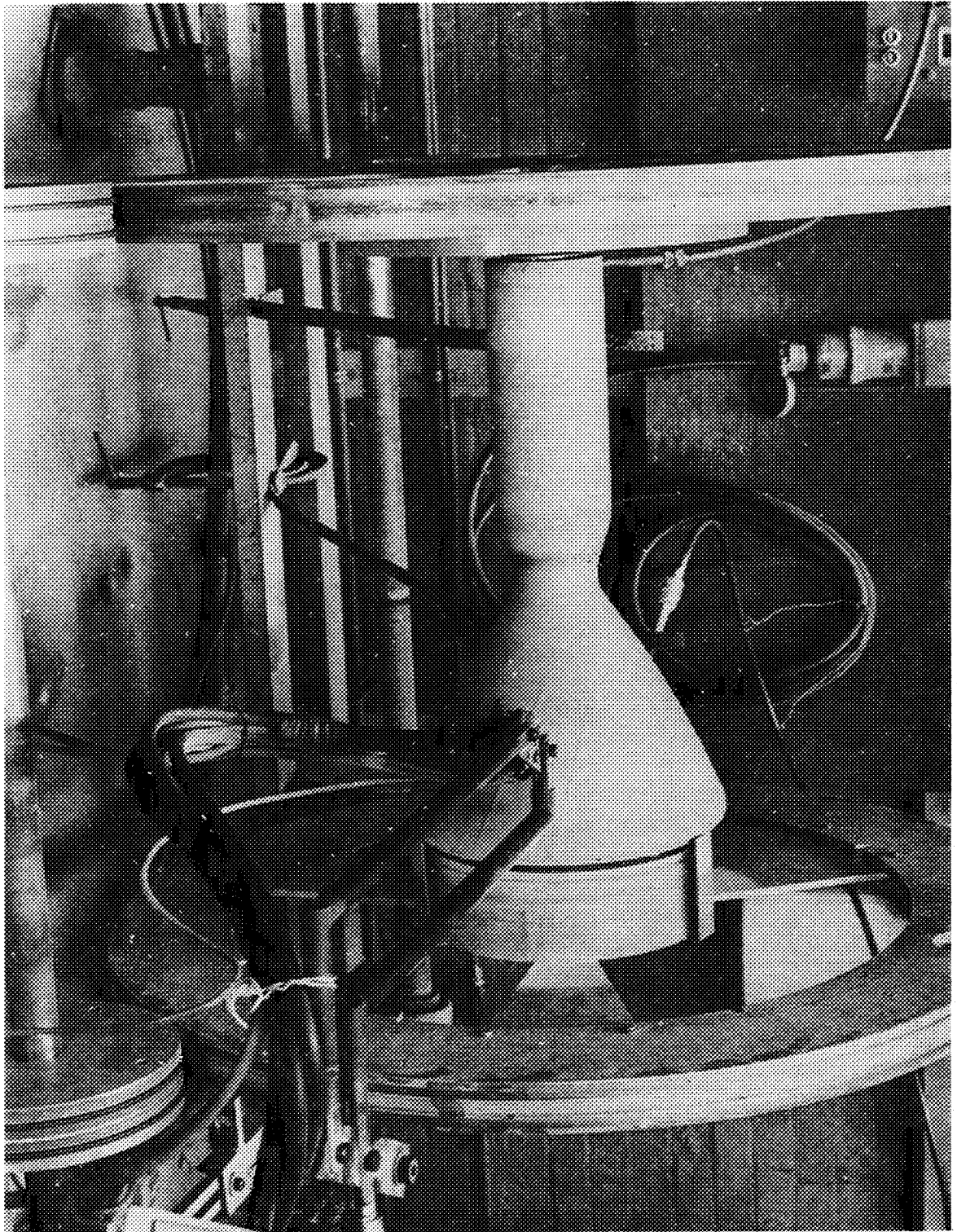
Figure 11. Plasma Arc Spraying 50% Complete

Figure 12. Plasma Arc Spraying 90% Complete

A

A

Graphite Mandrel

Step 1

Electroformed Nickel
Surface as Deposited

Contour Machine to
Inner Shell Thickness

Step 2

Vinyl Core Material –
Machined Contour & Rib Cavities
Rib Cavity
Inner Shell

Step 3

Electroformed Nickel
as Deposited

Contour Mach.

Vinyl

Step 4

Electroformed Nickel
As Deposited

Final Contour Mach.

Bond Line

Wax with Conductive
Coating (Vinyl Removed)

Step 5
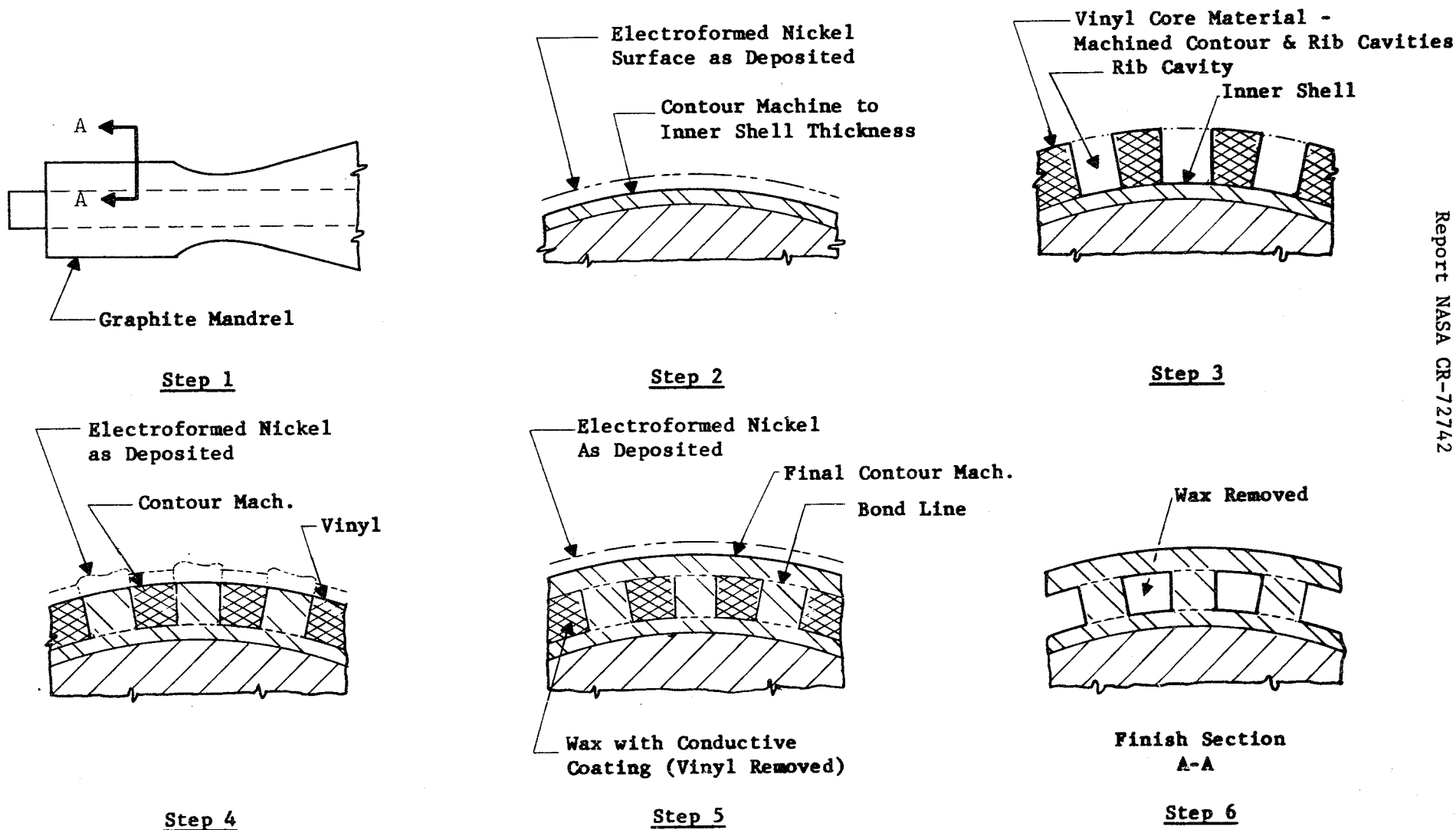
Wax Removed

Finish Section
A-A

Step 6

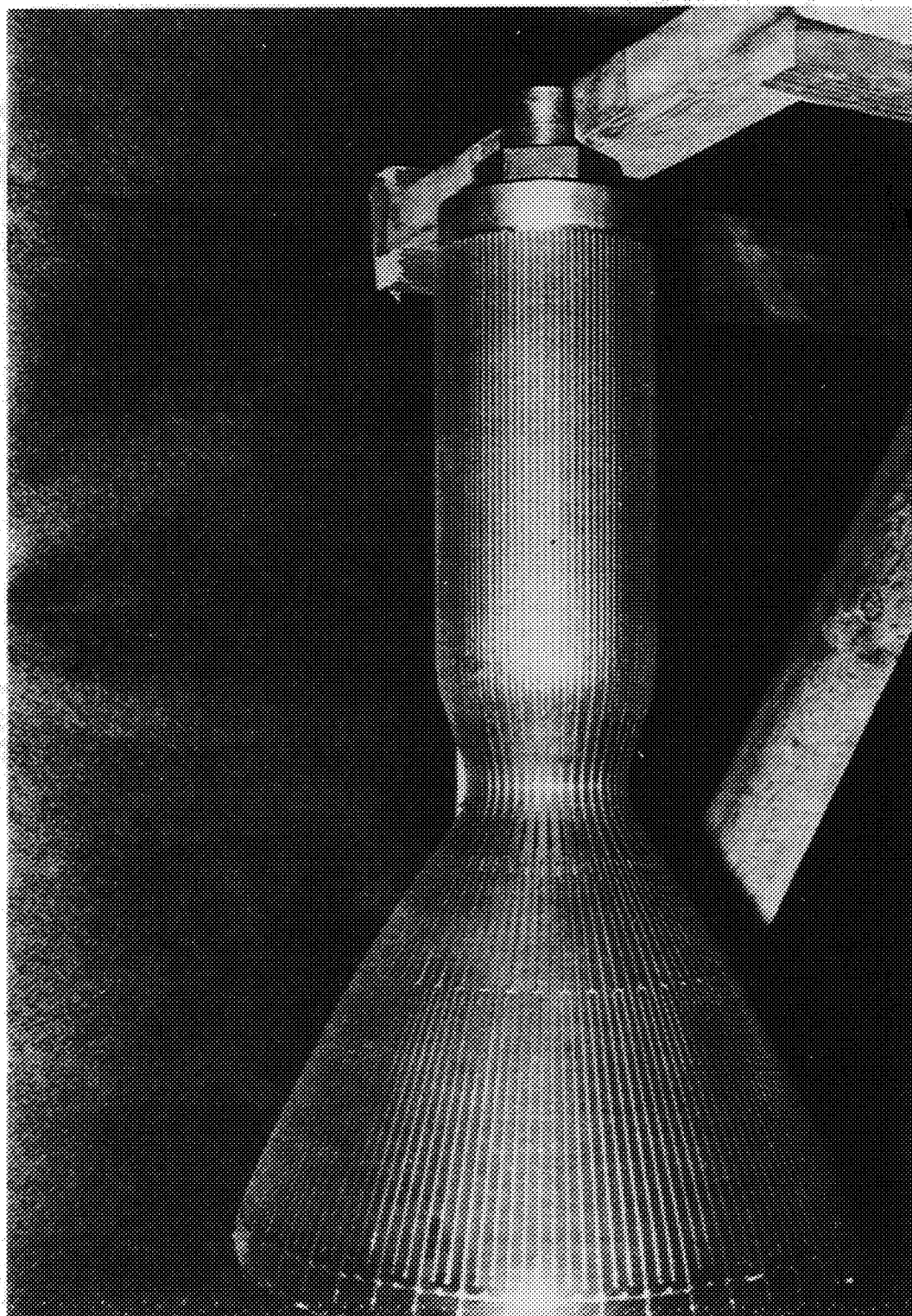Figure 13.   Process Steps – Formed Channels

Figure 14.   Mandrel with Ribs Cut in Vinyl
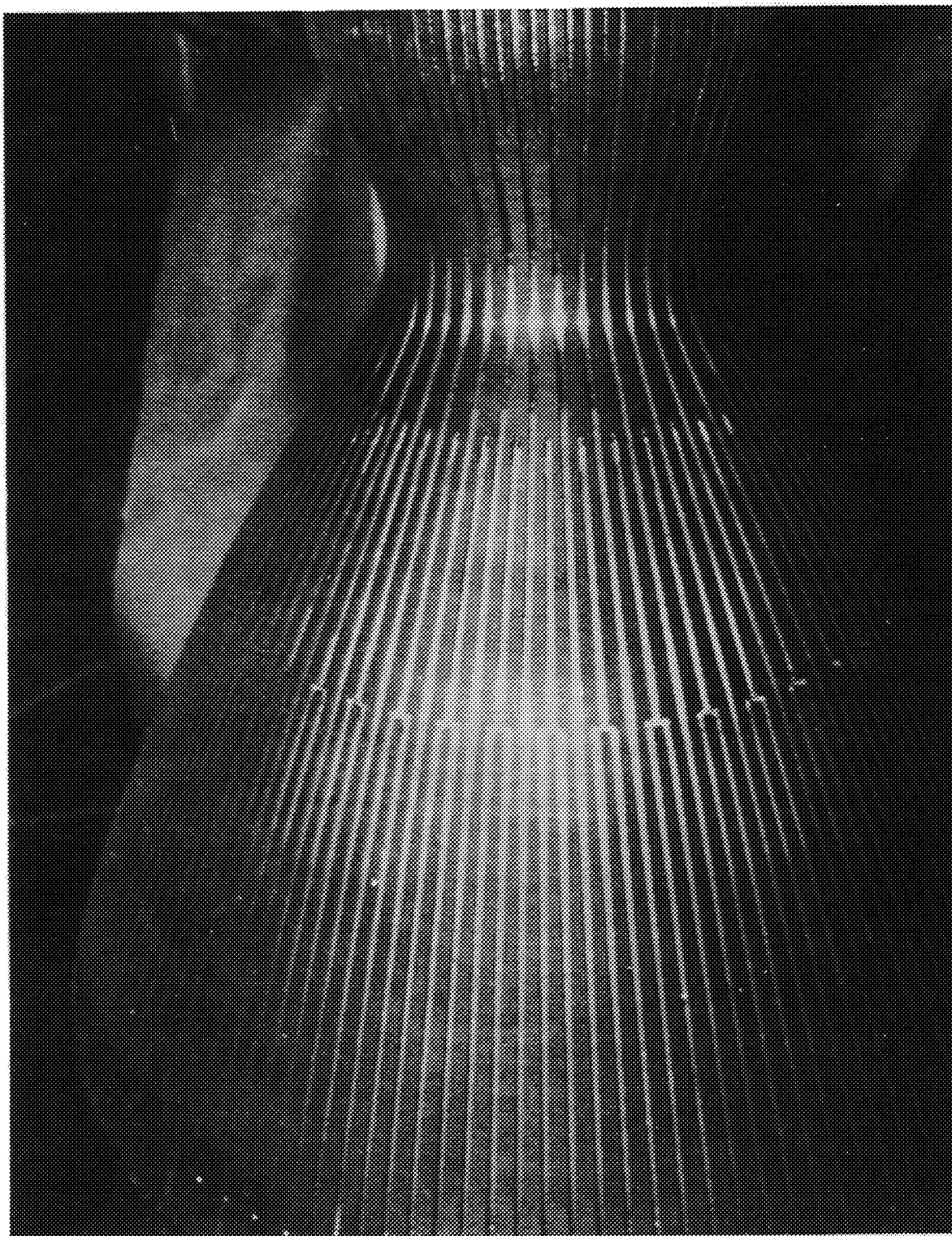
Figure 15. Vinyl Machining Results
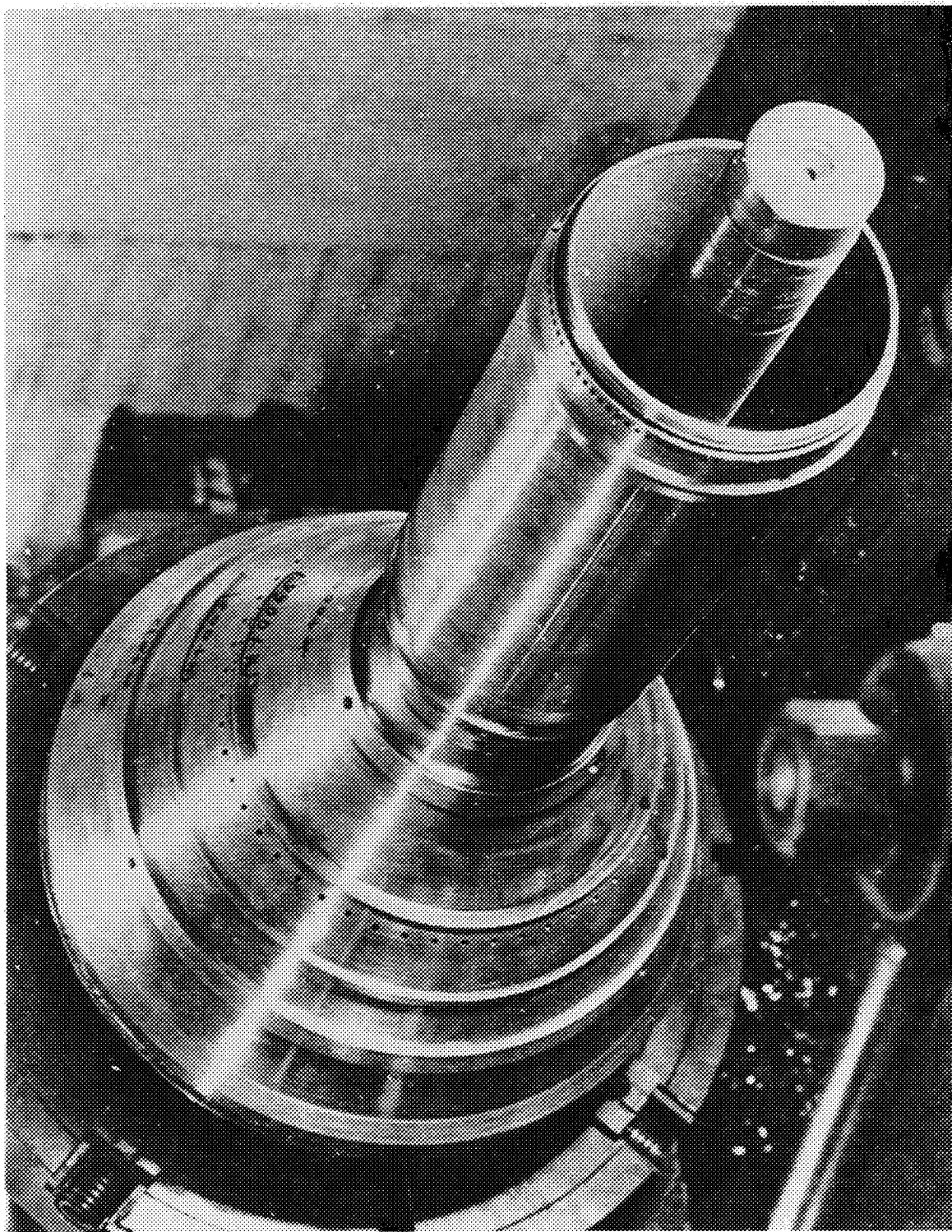
Figure 16. Dimensional Inspection

11. 400
dia

E. B. Weld

0. 140

0. 250

Figure 17. Joint Design - Inlet Manifold

Chamber ℄

E. B. Weld ⟶
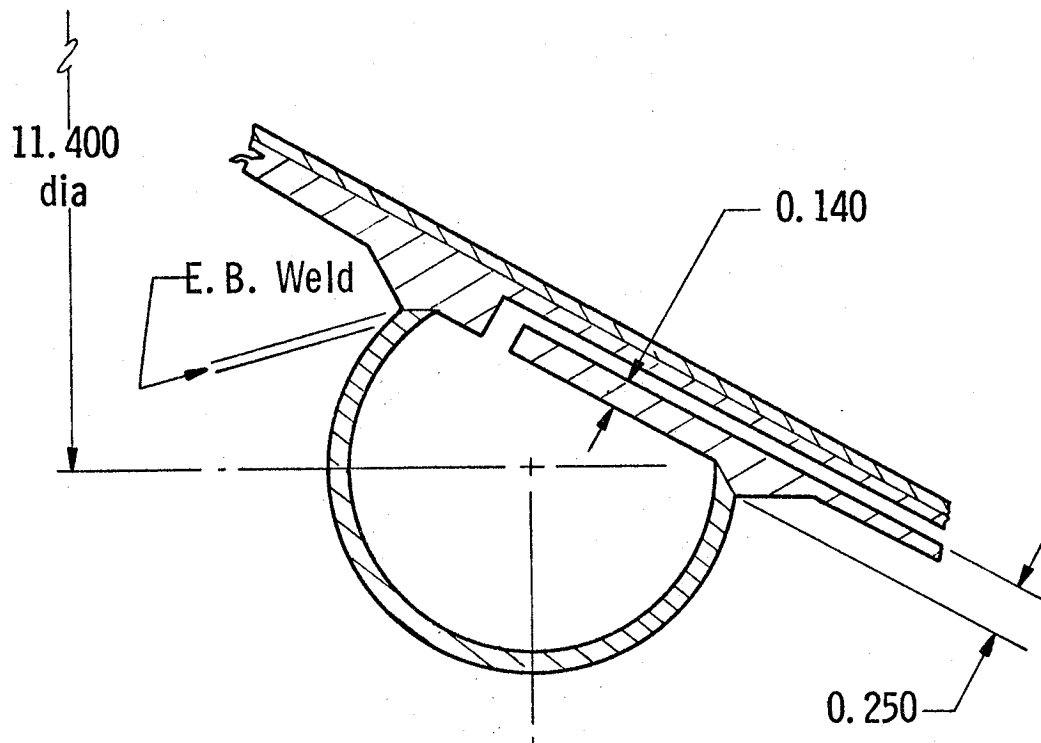
E. B. Weld
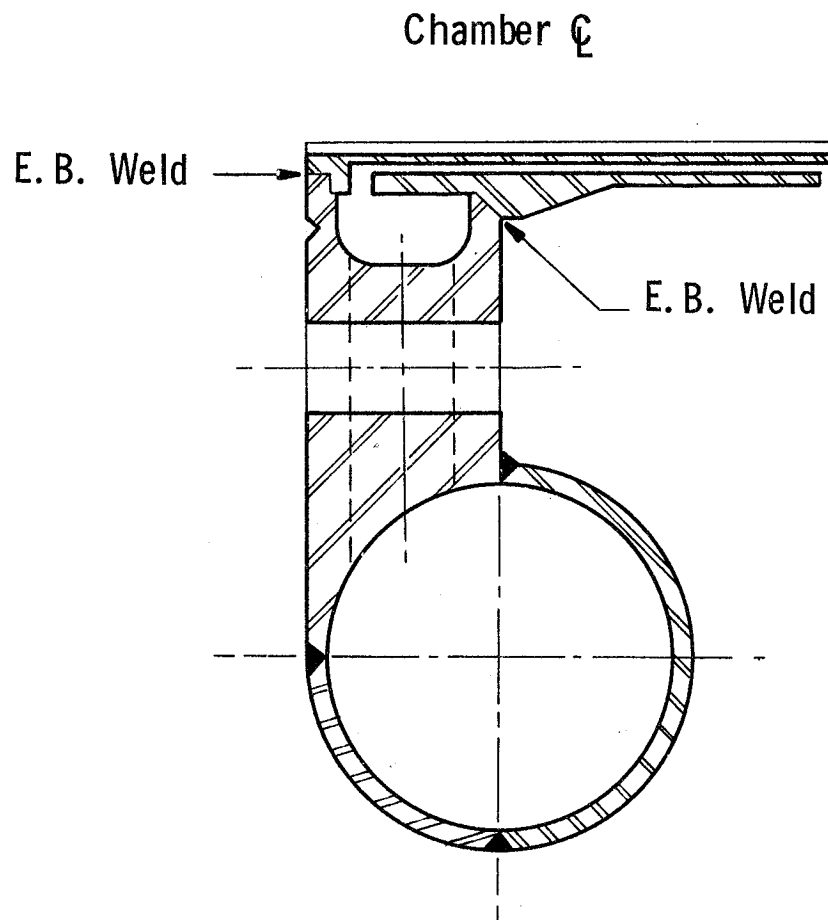
Figure 18. Joint Design - Outlet Manifold
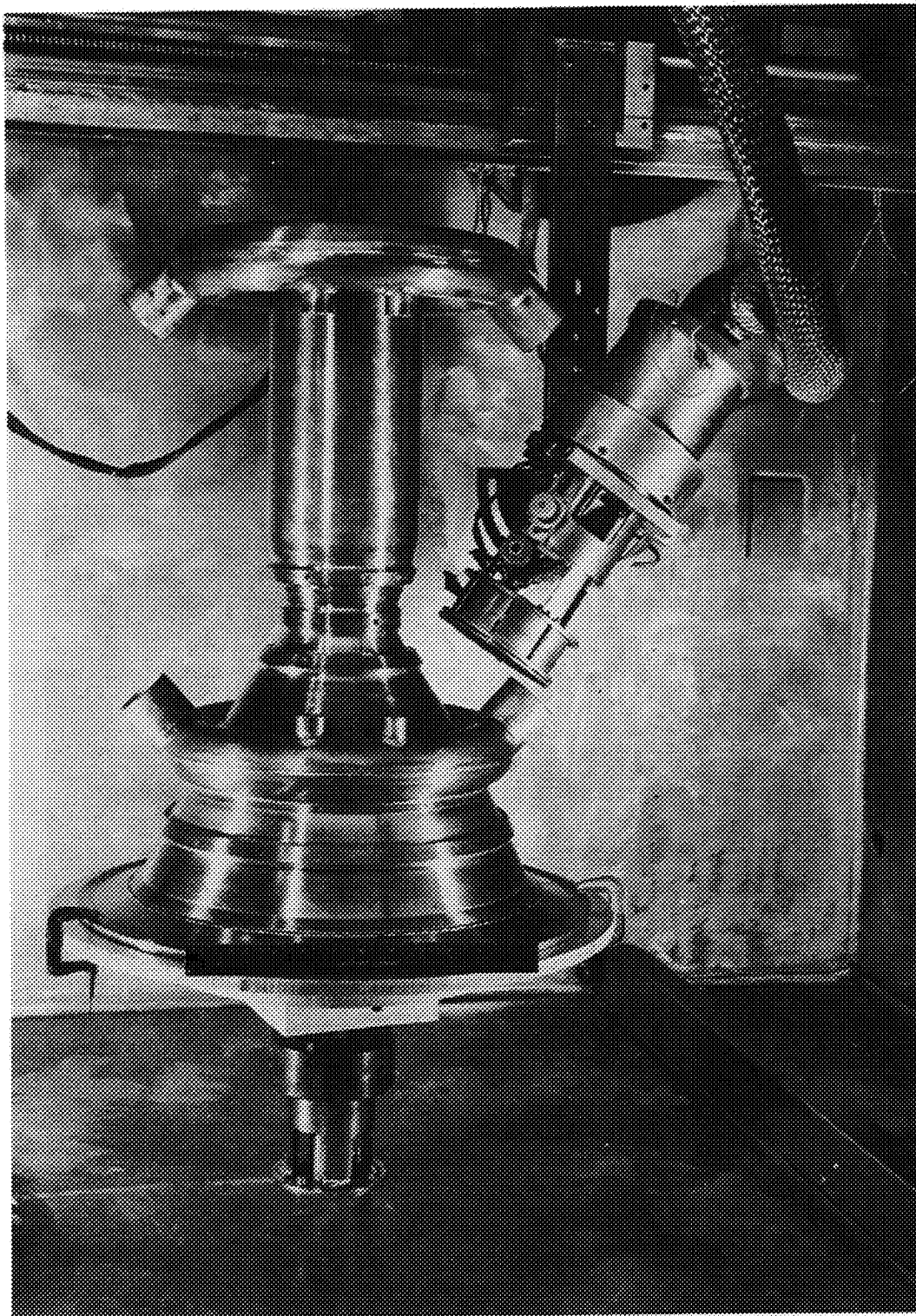
Figure 19. Electron Beam Welding Chamber, Inlet Manifold Forward Joint
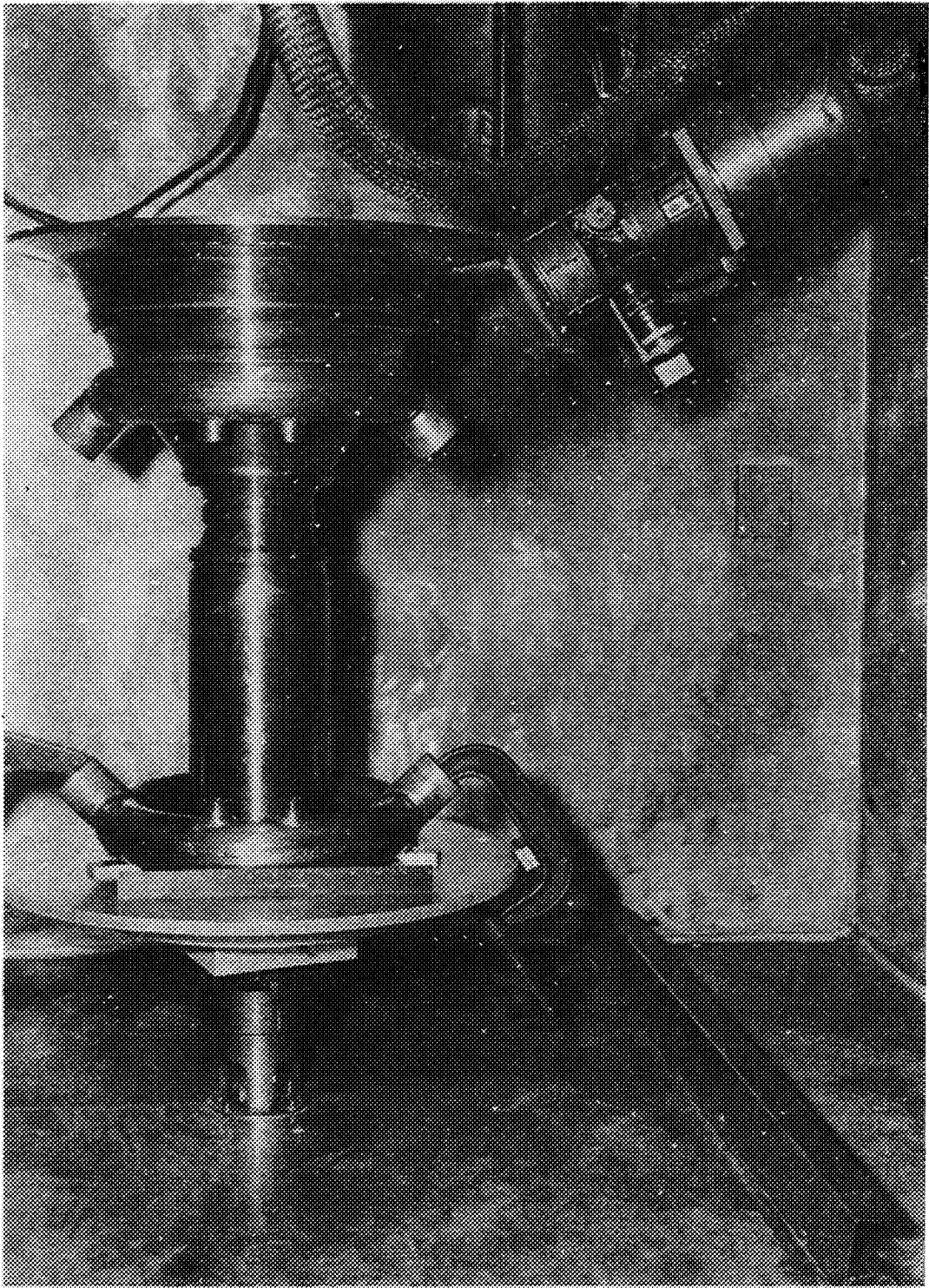
Figure 20. Electron Beam Welding Chamber, Inlet Manifold Aft Joint
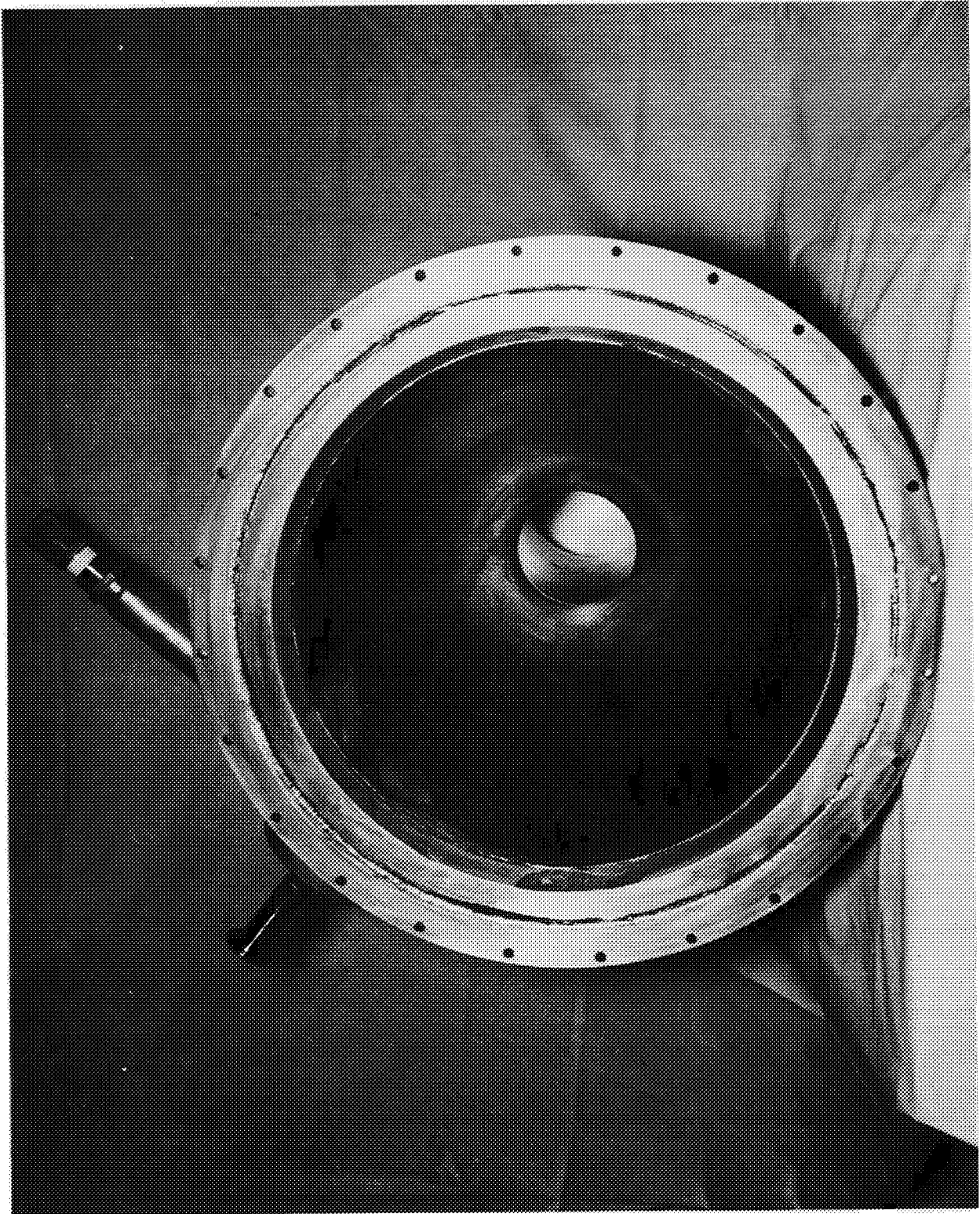
Figure 21. First Electroform Repair
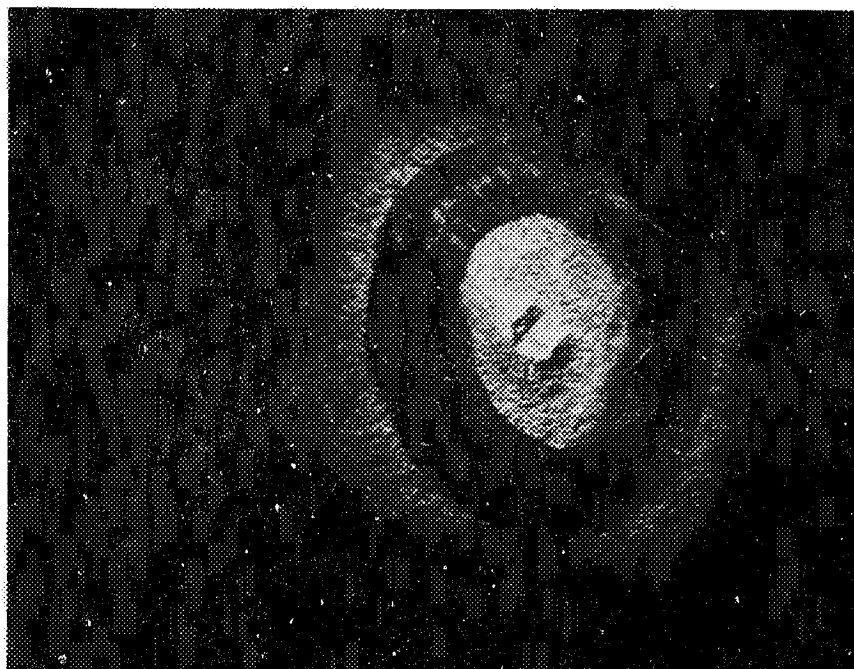
$2\frac{1}{2}$X

8X

Figure 22.   Leak in Chamber Wall - Single Hole
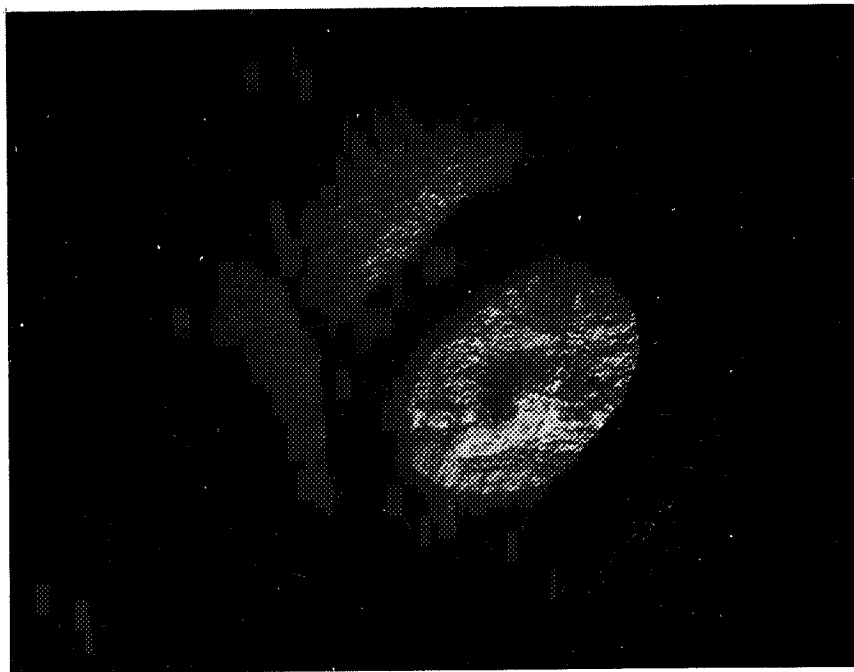
$2\frac{1}{2}$X
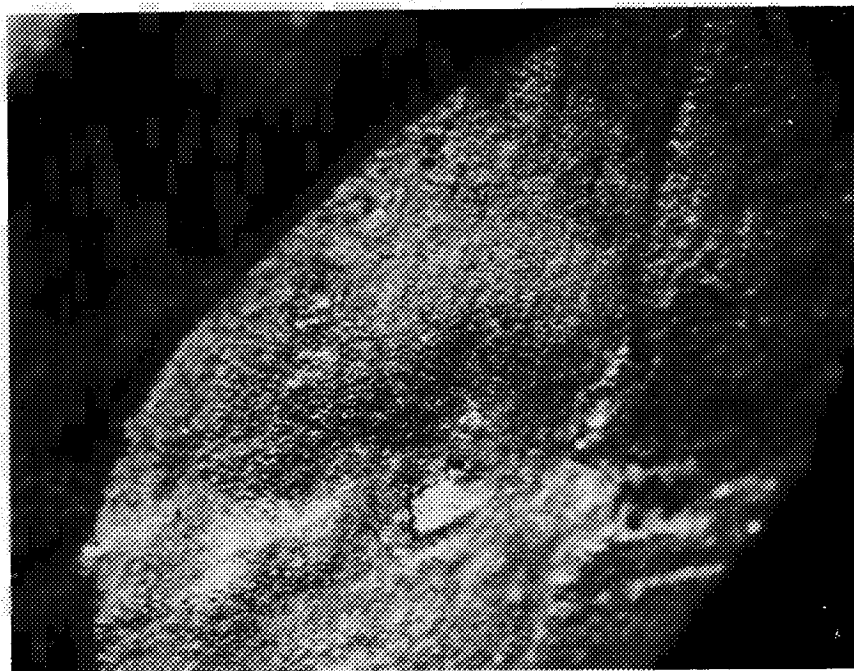
8X

Figure 23. Leak in Chamber Wall - Scattered Porosity
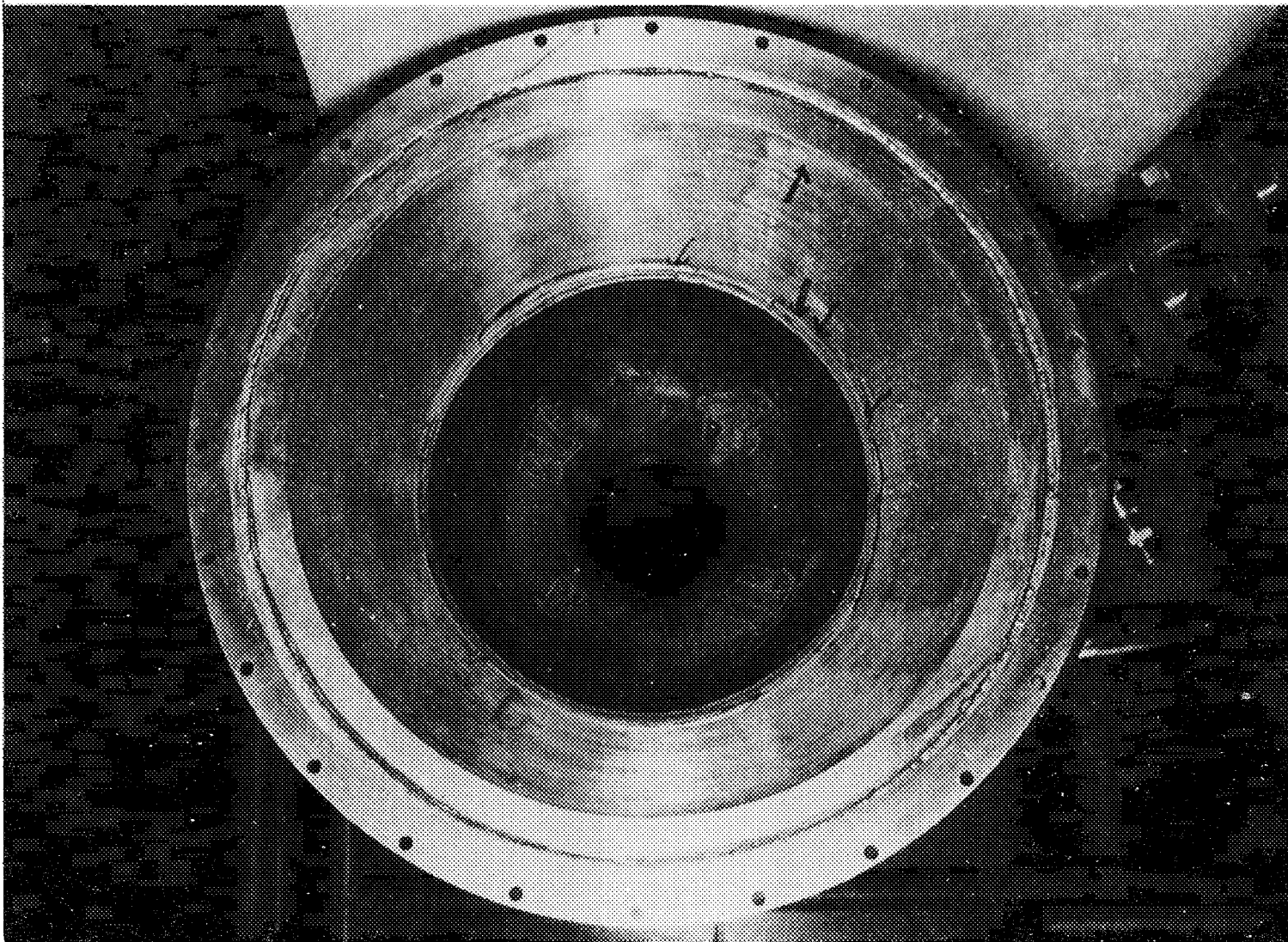
Figure 24.   Final Electroform Repair, Aft End, Showing Areas of Leakage

Figure 25. Thrust Chamber with Plumbing Attached

Figure 26. Wall Temperature Distributions

Figure 26. Wall Temperature Distributions

Report NASA CR-72742
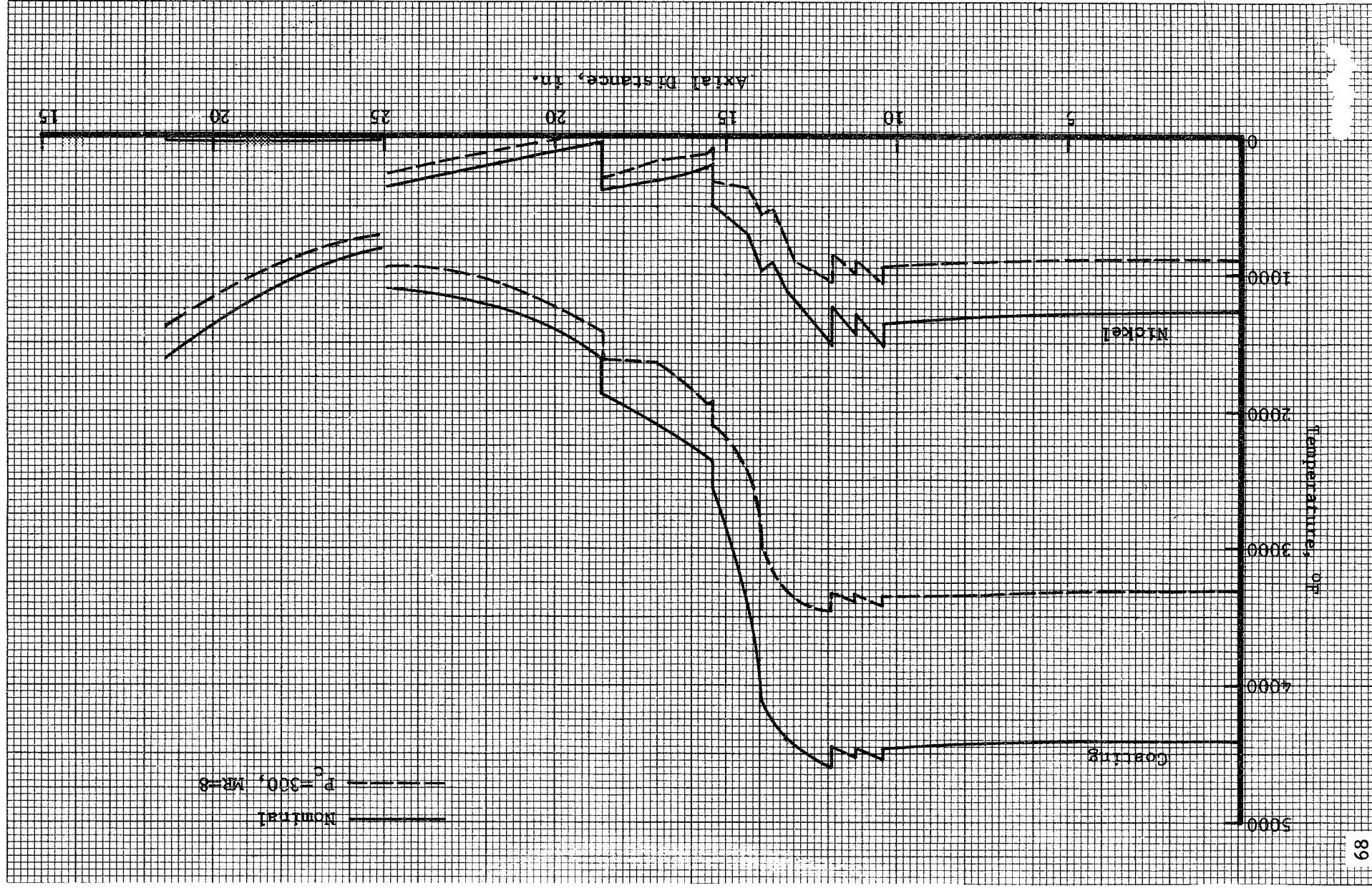
Figure 27. Heat Flux Distributions
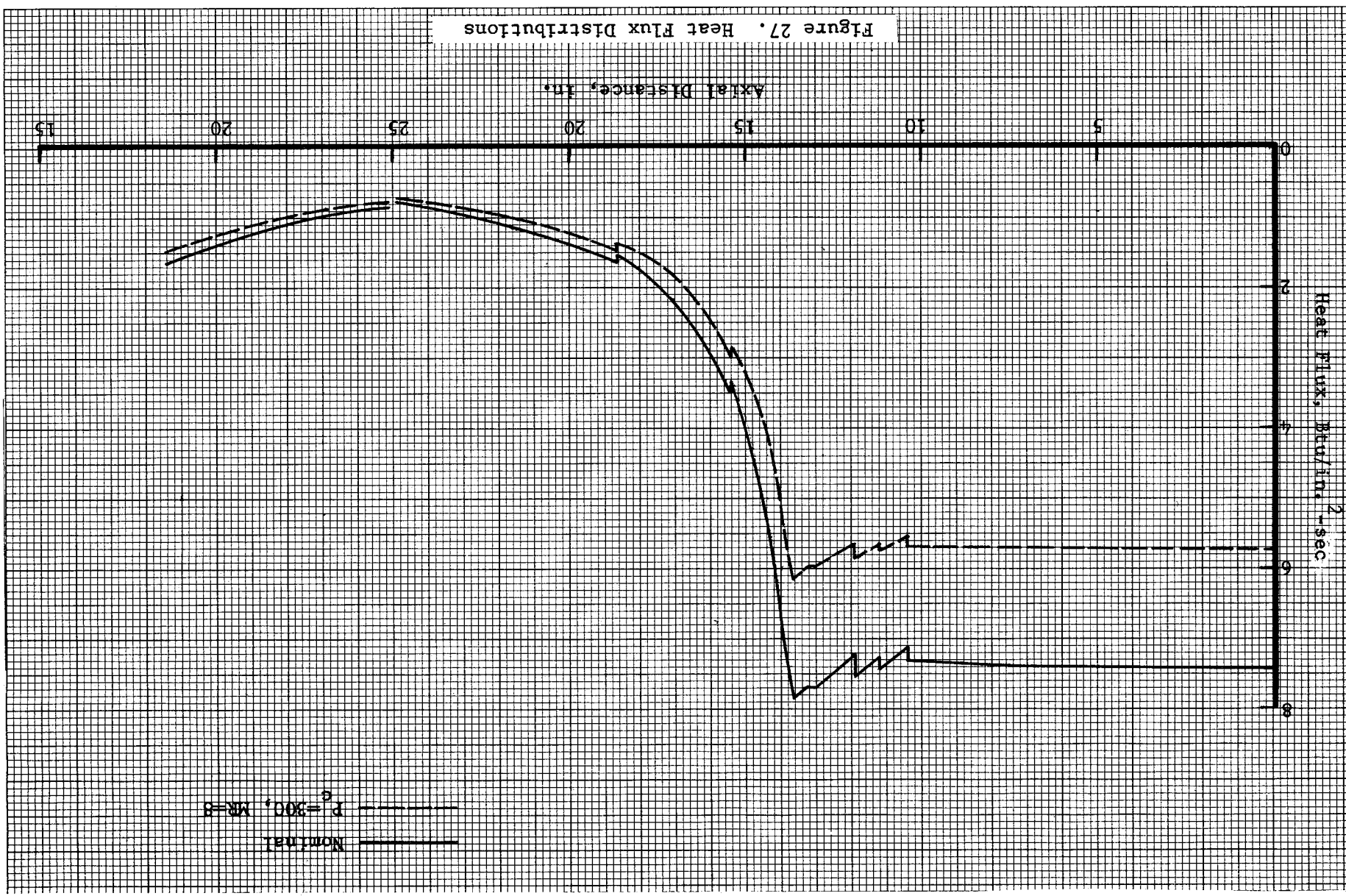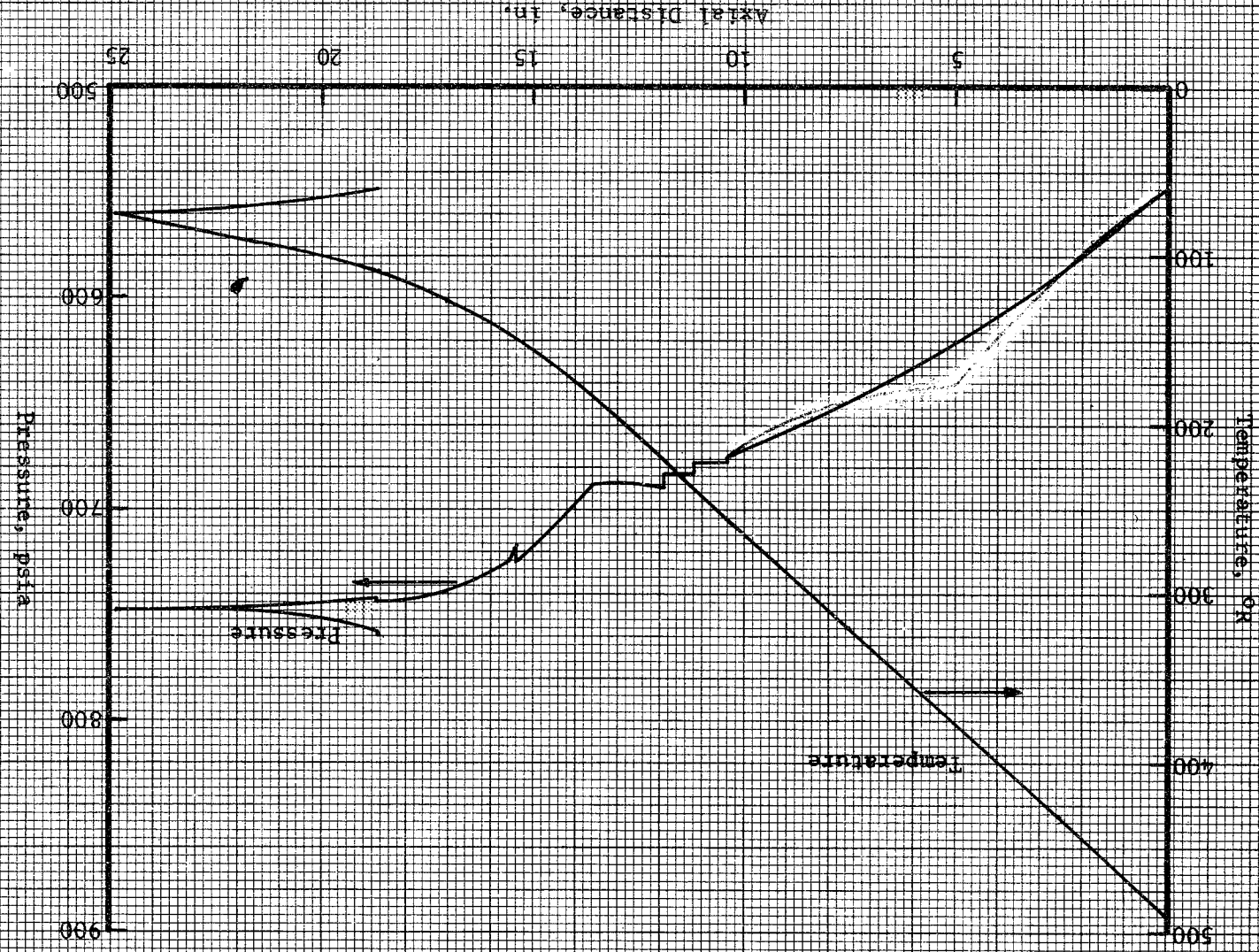
Axial Distance, in.

Heat Flux, Btu/in.²-sec

Nominal

$P_c = 300, MR = 8$

COOLANT CHANNEL
LINE OF OF SYMMETRY

ELECTROFORMED
NICKEL

HYDROGEN COOLANT
AT LOCAL P_B & T_B

$W/Zr\ O_2$

TUNGSTEN

RAD.   RAD.   CONV.

T_0 T_∞ HOT GAS TO LOCAL T_r
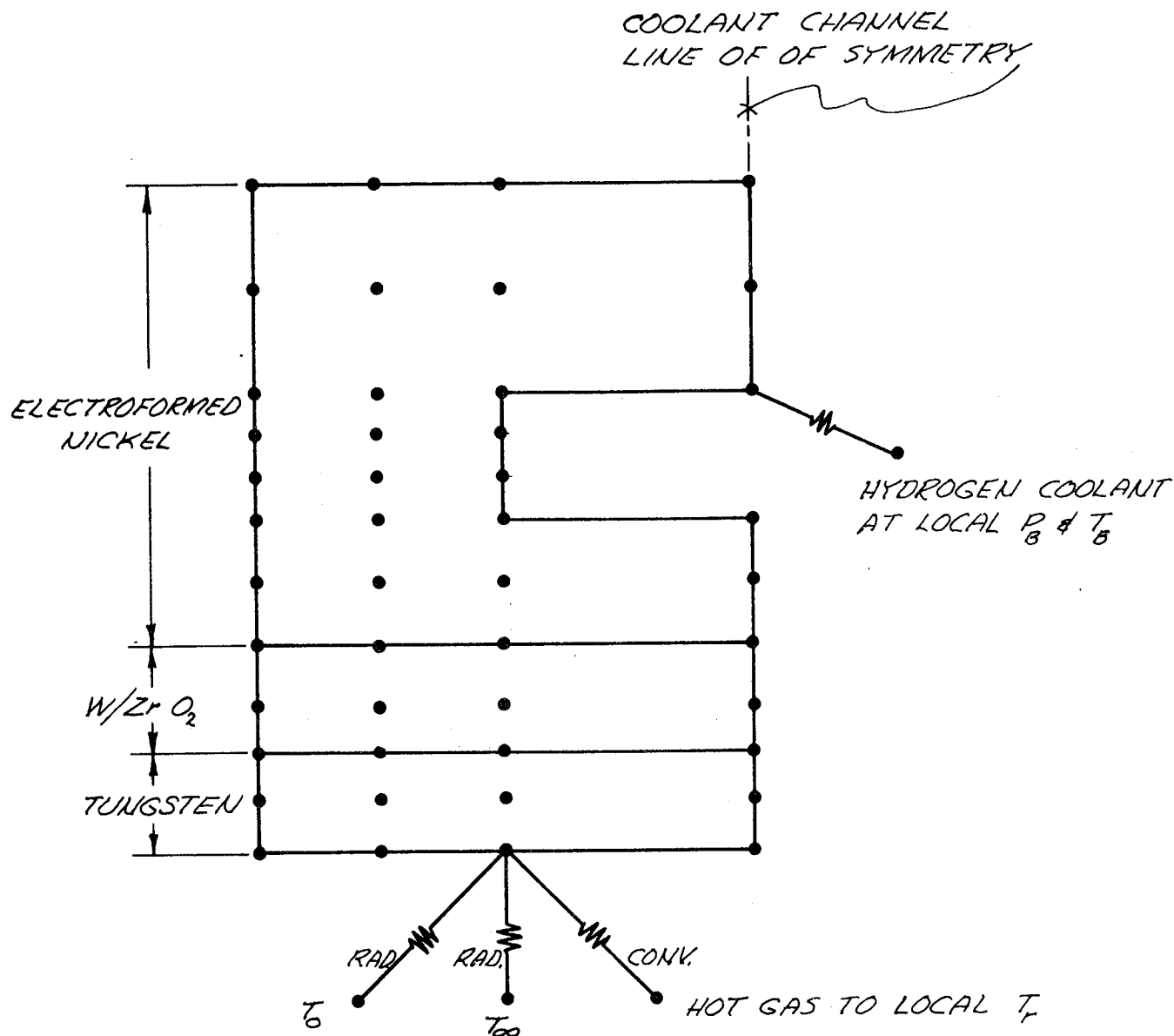
T_r = HOT GAS RECOVERY TEMPERATURE
T_∞ = HOT GAS FREE STREAM TEMPERATURE
T_0 = RADIATION SINK TEMPERATURE
P_B = COOLANT BULK PRESSURE
T_B = COOLANT BULK TEMPERATURE

Figure 29.   Thermal Model Node Network

```
**********
TIME   1.00000-01 DTIMEU   1.00000-01 CSGMIN(    1)    6.08430-04 DTMPCC
         TRANSIENT SOLUTION FOR AXIAL DISTANCE= 13.65IN.
                     48. NO. OF COOLANT CHANNELS


            -----   ************** NICKEL ******************
              *       *                                    *
              *       *-398.8    -399.0    -399.5    -402.3*
THICK = .060  *       *                                    *
              *       *-397.4    -397.8    -398.7    -402.4*
              *       *                                    *
              *       *-392.2    -393.2    -396.4    -402.9*
            -----     *                         ************
              *       *-384.1    -384.7    -386.4*
THICK = .060  *       *                         *  -410.0 BULK TEMP-DEG-F
              *       *-372.7    -373.0    -374.3*
            -----     *                         ************
              *       *-358.1    -357.5    -354.9    -345.5*
THICK = .030  *       *                                    *
              *       *-346.3    -345.8    -344.2    -337.1*
              *       *                                    *
            -----     *-333.4**** -332.9**** -331.6**** -325.4* INTERFACE
              *       *                                    *
THICK = .037  *       *   -.1       .4       2.4       2.6*
              *       *                                    *
            -----     * 456.6****  456.6****  457.0****  457.1* INTERFACE
              *       *                                    *
              *       * 482.4     482.4     482.5     483.0*
THICK = .030  *       *                                    *
              *       * 518.4     518.3     517.4     519.1*
            -----     ************** TUNGSTEN ****************


            *--------   .0450--------------*- .0890--*


              RECOVERY TEMP = 7045.0 DEG-F

                GAS TEMP = 6621.1 DEG-F

                HG=   .00087 BTU/IN-SEC-F
                HL=   .01176 BTU/IN-SEC-F
                HL=   .01176 BTU/IN-SEC-F
                HL=   .01176 BTU/IN-SEC-F
                HL=   .01176 BTU/IN-SEC-F
                HL=   .01176 BTU/IN-SEC-F
                HL=   .01176 BTU/IN-SEC-F
        PB=   755.9PSI  PV= 3.9706 PSI PF=  .15369 PSI
        QIN =  49.440   QOUT =   6.577   QRAD =    1.567


        TOTAL PV=    .00PSI    TOTAL PF=    .00 PSI
      AF        DE       VELOCITY  VISCOSITY  DENSITY    RE
      SQ IN     IN        IN/SEC    LB/FT-SEC  LB/FT3    --

      .5126     .0897     92.228    .7671-05    4.325    .38891+06


          ZRO2 TBAR =    65.87   ZRO2 DEL-T = 782.519
```
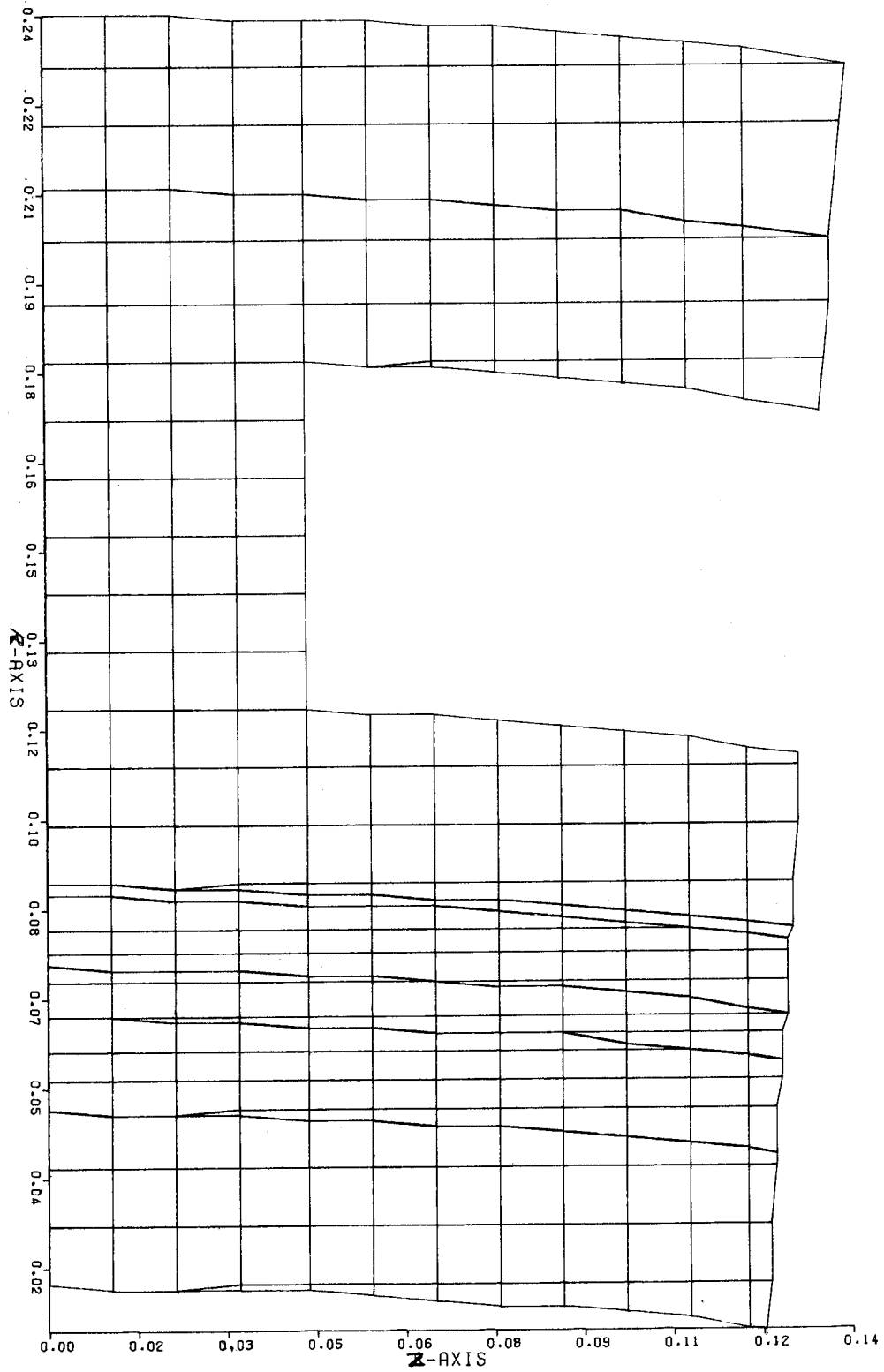
Figure 30. Typical Computer Printout Sheet

Figure 31. Computer Plot of Grid – Throat Section
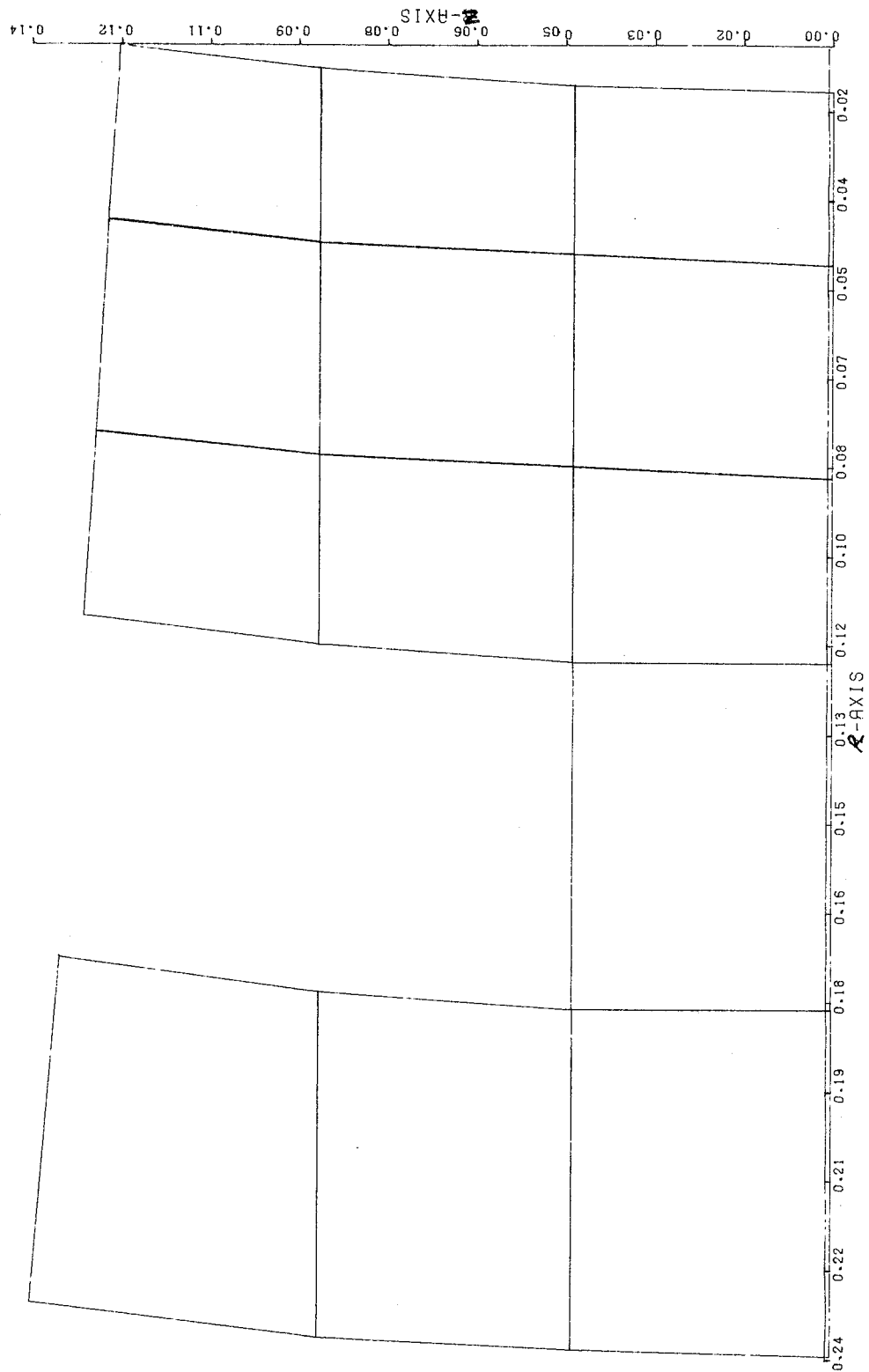
Figure 32. Grid for Computer Solution – Throat Section

STEPPED STARTUP AND SHUTDOWN
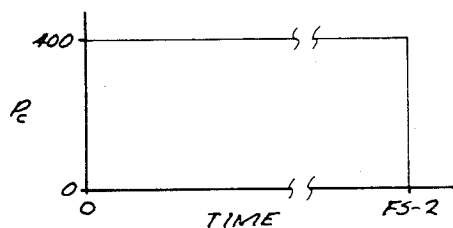
0.3 sec RAMPED STARTUP AND SHUTDOWN
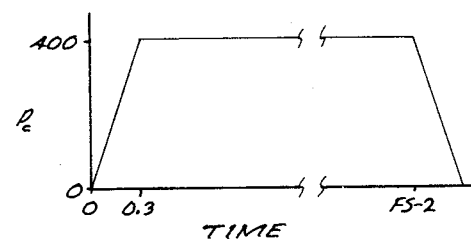
$P_c = 300$ STEPPED STARTUP
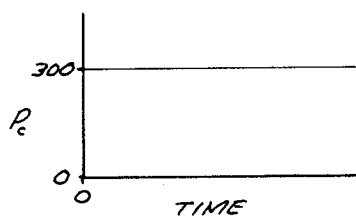
2.0 sec RAMPED STARTUP
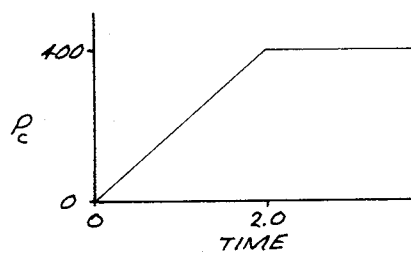
STEPPED RAMP STARTUP
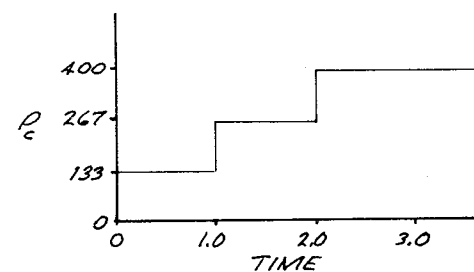
NOTE: P_c = CHAMBER PRESSURE, PSIA
TIME IN SEC.

Figure 33.   Injector Startup and Shutdown Cycles

TUNGSTEN-ZIRCONIA TEMPERATURE CHANGE AT
THE THROAT FOR VARIOUS STARTUP AND
SHUTDOWN CYCLES.
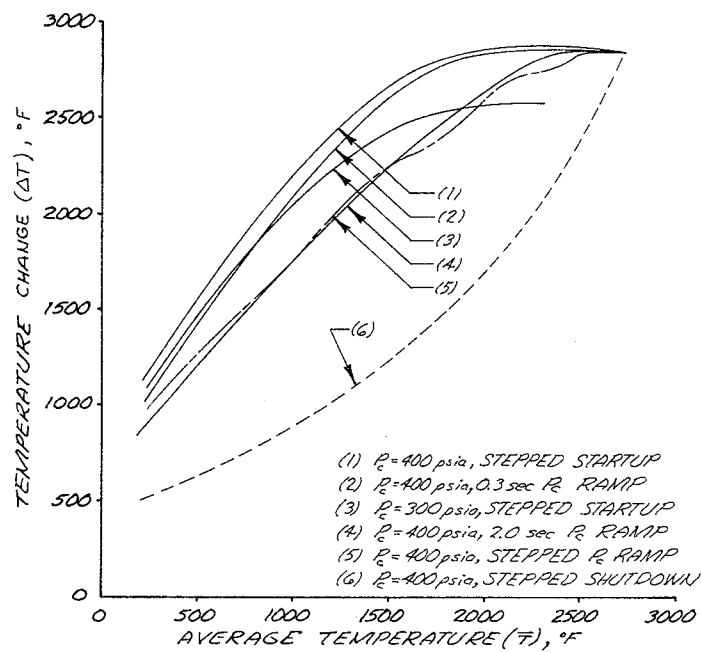
TUNGSTEN-ZIRCONIA TEMPERATURE
CHANGE DEPENDENCE ON COMBUSTION
RAMP TIME.

(1) P_c = 400 psia, STEPPED STARTUP
(2) P_c = 400 psia, 0.3 sec P_c RAMP
(3) P_c = 300 psia, STEPPED STARTUP
(4) P_c = 400 psia, 2.0 sec P_c RAMP
(5) P_c = 400 psia, STEPPED P_c RAMP
(6) P_c = 400 psia, STEPPED SHUTDOWN
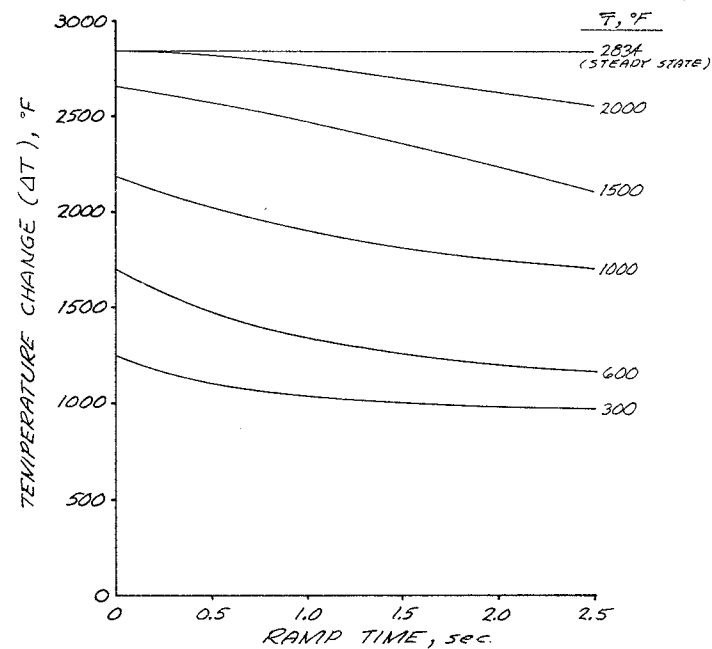
Figure 34.   Combustor Ramping Effects on Chamber Throat Temperatures
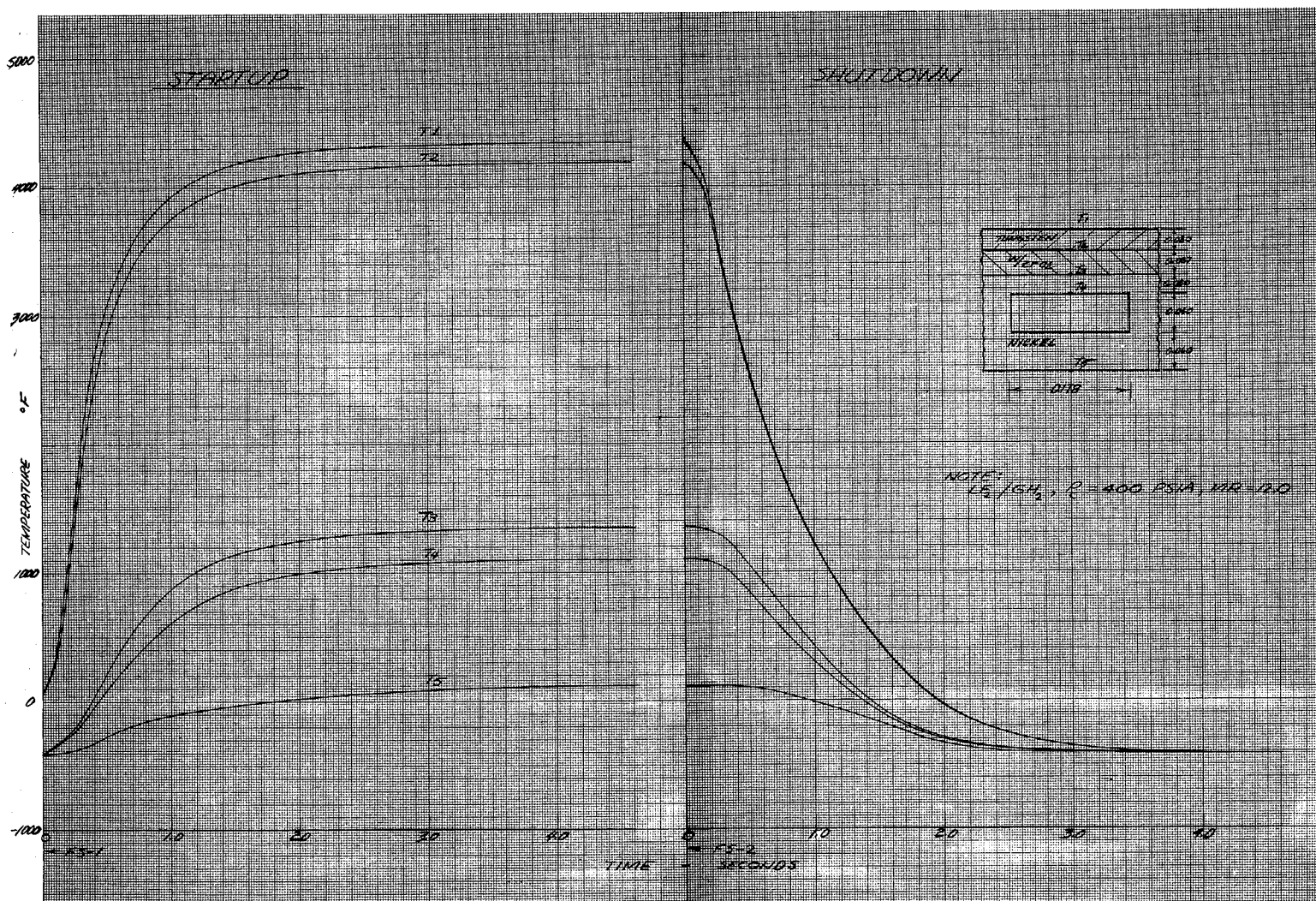
Figure 35. Temperature Response at the Throat for Stepped Combustion
Startup and Shutdown

Throat Section

$P_c = 400$ psi
$P_T = 730$ psi

78

Figure 37. Hoop Stresses, Throat Section – Two Second Ramp Start
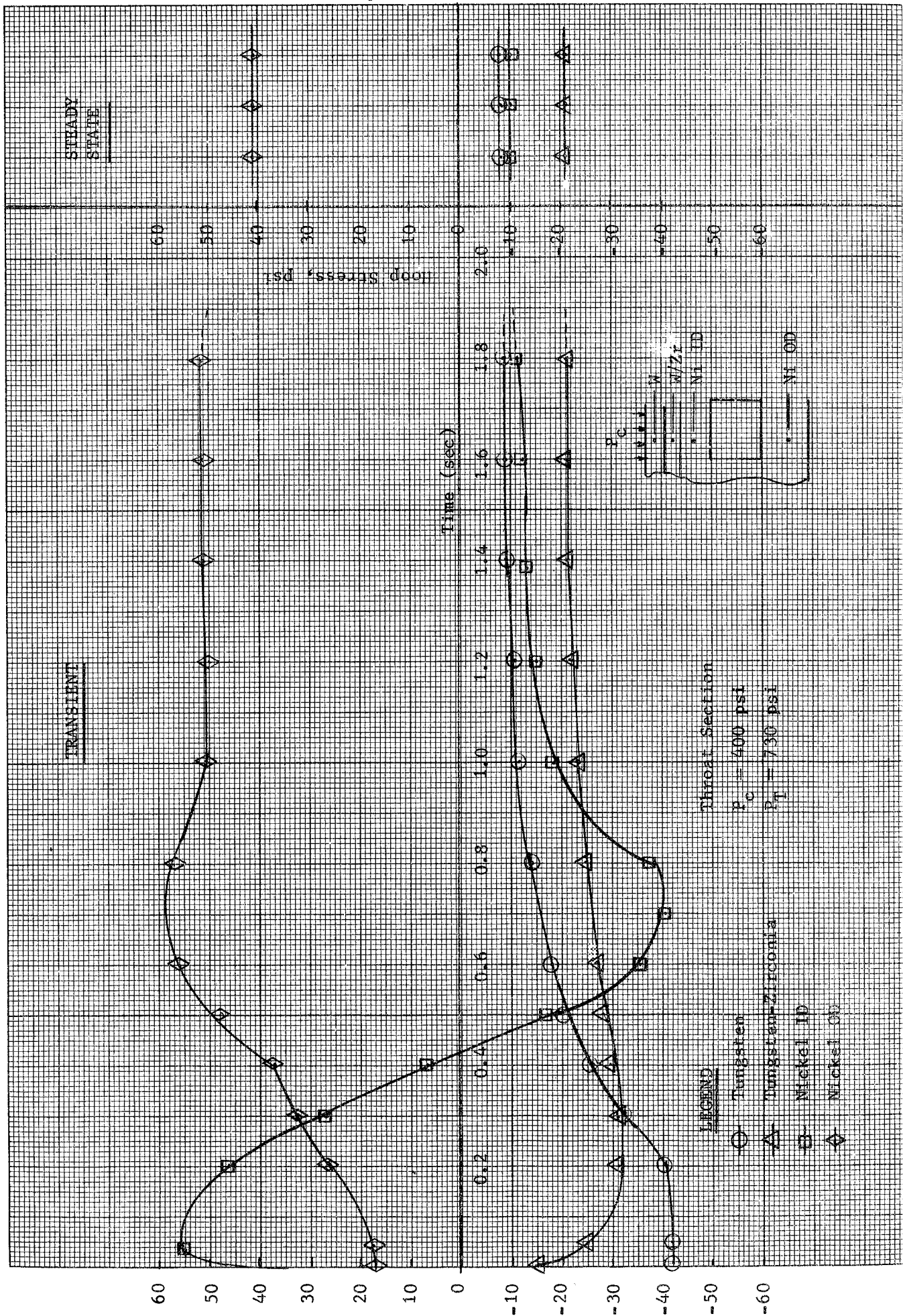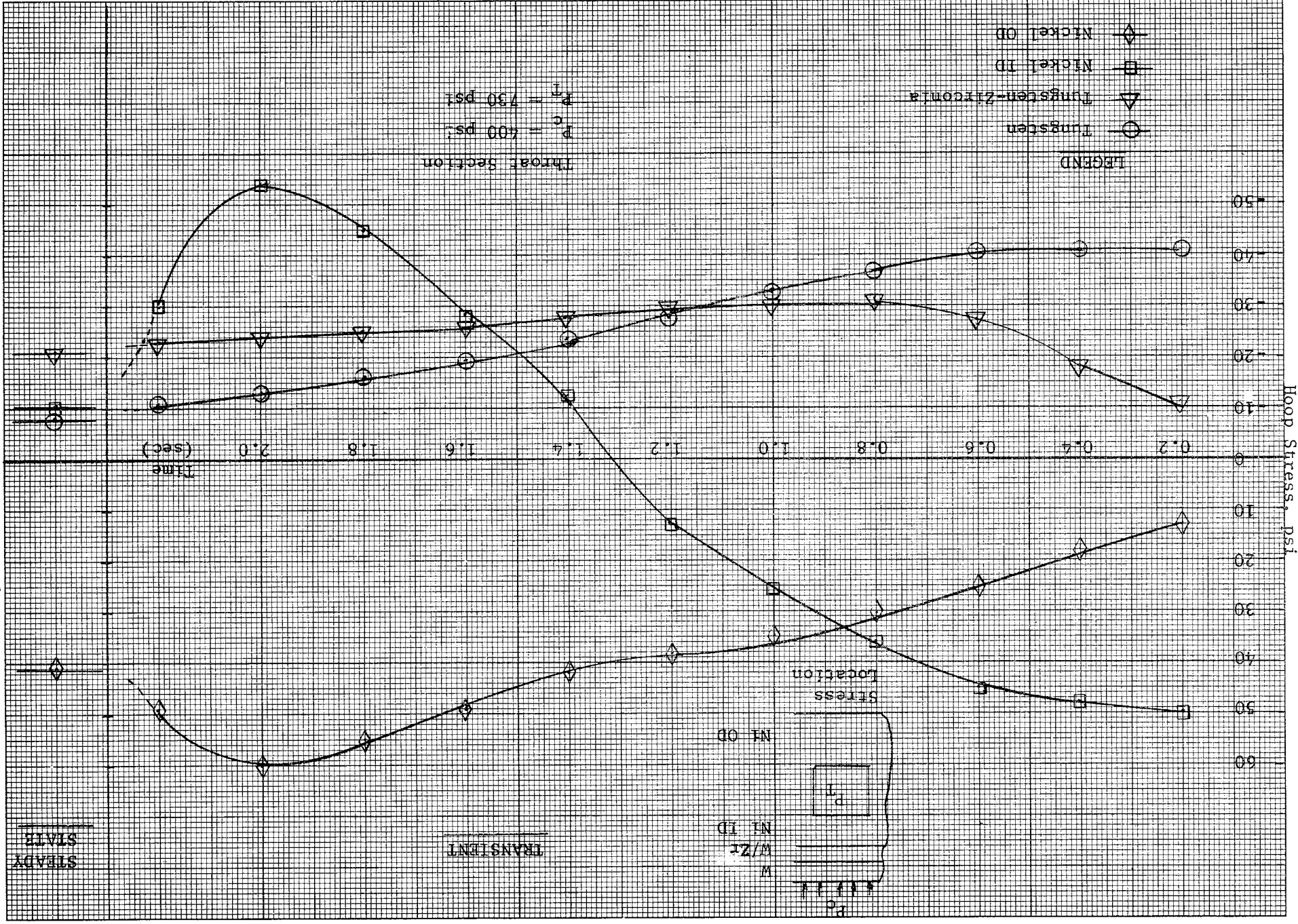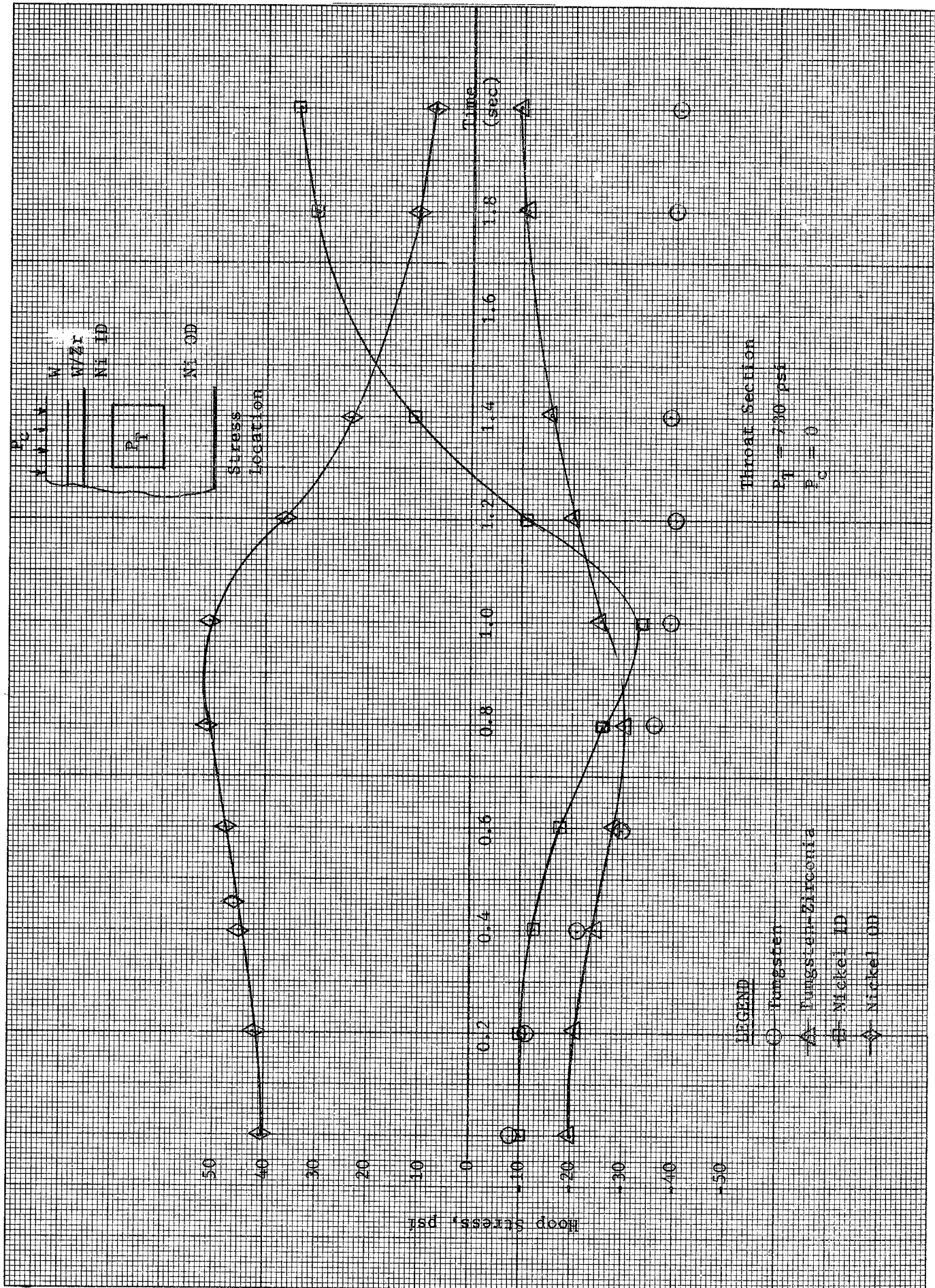
DISTRIBUTION LIST

Report Copies R D	Recipient	Designee

National Aeronautics & Space Administration
Lewis Research Center
21000 Brookpark Road
Cleveland, Ohio 44135

R D	Recipient
1	Attn: Contracting Officer, MS 500-313
5	Liquid Rocket Technology Branch, MS 500-209
1	Technical Report Control Office, MS 5-5
1	Technology Utilization Office, MS 3-16
2	AFSC Liaison Office, 501-3
2	Library
1	Office of Reliability & Quality Assurance, MS 500-111
1	D. L. Nored, Chief, LRTB, MS 500-209
10	R. A. Duscha, Project Manager, MS 500-209
1	E. W. Conrad, MS 500-204
1	J. W. Gregory, MS 500-209
1	J. M. Kazaroff, MS 500-203
1	A. N. Curren, MS 500-204

2 Chief, Liquid Experimental Engineering, RPX
Office of Advanced Research & Technology
NASA Headquarters
Washington, D.C. 20546

2 Chief, Liquid Propulsion Technology, RPL
Office of Advanced Research & Technology
NASA Headquarters
Washington, D.C. 20546

1 Director, Launch Vehicles & Propulsion, SV
Office of Space Science & Applications
NASA Headquarters
Washington, D.C. 20546

1 Chief, Environmental Factors & Aerodynamics
Code RV-1
Office of Advanced Research & Technology
NASA Headquarters
Washington, D.C. 20546

DISTRIBUTION LIST (cont.)

Report Copies R D	Recipient	Designee
1	Chief, Space Vehicles Structures Office of Advanced Research & Technology NASA Headquarters Washington, D.C. 20546	
1	Director, Advanced Manned Missions, MT Office of Manned Space Flight NASA Headquarters Washington, D.C. 20546	
6	NASA Scientific & Technical Information Facility P. O. Box 33 College Park, Maryland 20740	
1	Director, Technology Utilization Division Office of Technology Utilization NASA Headquarters Washington, D.C. 20546	
1	National Aeronautics & Space Administration Ames Research Center Moffett Field, California 94035 Attn: Library	Hans M. Mark Mission Analysis Division
1	National Aeronautics & Space Administration Flight Research Center P. O. Box 273 Edwards, California 93523 Attn: Library	
1	National Aeronautics & Space Administration Goddard Space Flight Center Greenbelt, Maryland 20771 Attn: Library	Merland L. Moseson, Code 620
1	National Aeronautics & Space Administration John F. Kennedy Space Center Cocoa Beach, Florida 32931 Attn: Library	Dr. Kurt H. Debus
1	National Aeronautics & Space Administration Langley Research Center Langley Station Hampton, Virginia 23365 Attn: Library	E. Cortwright Director

DISTRIBUTION LIST (cont.)

Report Copies R D	Recipient	Designee
1	National Aeronautics & Space Administration Manned Spacecraft Center Houston, Texas 77001 Attn: Library	J. G. Thiobodaux, Jr. Chief Propulsion & Power Division
1	National Aeronautics & Space Administration George C. Marshall Space Flight Center Huntsville, Alabama 35812 Attn: Library	Hans G. Paul Leon J. Hastings James Thomas Dale Burrows I. G. Yates Clyde Nevins J. Blumrich
1	Jet Propulsion Laboratory 4800 Oak Grove Drive Pasadena, California 91103 Attn: Library	Hunry Burlage, Jr. Duane Dipprey
1	Defense Documentation Center Cameron Station Building 5 5010 Duke Street Alexandria, Virginia 22314 Attn: TISIA	
1	Office of the Director of Defense Research & Engineering Washington, D.C. 20301 Attn: Office of Asst. Dir. (Chem. Technology)	
1	RTD (RTNP) Bolling Air Force Base Washington, D.C. 20332	
1	Arnold Engineering Development Center Air Force Systems Command Tullahoma, Tennessee 37389 Attn: Library	Dr. H. K. Doetsch
1	Advanced Research Projects Agency Washington, D.C. 20525 Attn: Library	

DISTRIBUTION LIST (cont.)

Report Copies R D	Recipient	Designee
1	Aeronautical Systems Division Air Force Systems Command Wright-Patterson Air Force Base, Dayton, Ohio Attn: Library	D. L. Schmidt Code ARSCNC-2
1	Air Force Missile Test Center Patrick Air Force Base, Florida Attn: Library	L. J. Ullian
1	Air Force Systems Command Andrews Air Force Base Washington, D.C. 20332 Attn: Library	Capt. S. W. Bowen SCLT
1 1	Air Force Rocket Propulsion Laboratory (RPR) Edwards, California 93523 Attn: Library	Donald Penn Robert Wiswell
1	Air Force Rocket Propulsion Laboratory (RPM) Edwards, California 93523 Attn: Library	
1	Air Force FTC (FTAT-2) Edwards Air Force Base, California 93523 Attn: Library	Donald Ross
1	Air Force Office of Scientific Research Washington, D.C. 20333 Attn: Library	SREP, Dr. J. F. Masi
1	Space & Missile Systems Organization Air Force Unit Post Office Los Angeles, California 90045 Attn: Technical Data Center	
1	Office of Research Analyses (OAR) Holloman Air Force Base, New Mexico 88330 Attn: Library RRRD	
1	U. S. Air Force Washington, D.C. Attn: Library	Col. C. K. Stambaugh, Code AFRST

DISTRIBUTION LIST (cont.)

Report Copies R D	Recipient	Designee
1	Commanding Officer U. S. Army Research Office (Durham) Box CM, Duke Station Durham, North Carolina 27706 Attn: Library	
1	U. S. Army Missile Command Redstone Scientific Information Center Redstone Arsenal, Alabama 35808 Attn: Document Section	Dr. W. Wharton
1	Bureau of Naval Weapons Department of the Navy Washington, D.C. Attn: Library	J. Kay, Code RTMS-41
1	Commander U. S. Naval Missile Center Point Mugu, California 93041 Attn: Technical Library	
1	Commander U. S. Naval Weapons Center China Lake, California 93557 Attn: Library	
1	Commanding Officer Naval Research Branch Office 1030 E. Green Street Pasadena, California 91101 Attn: Library	
1	Director (Code 6180) U. S. Naval Research Laboratory Washington, D.C. 20390 Attn: Library	H. W. Carhart J. M. Krafft
1	Picatinny Arsenal Dover, New Jersey 07801 Attn: Library	I. Forsten

DISTRIBUTION LIST (cont.)

Report Copies R D	Recipient	Designee
1	Air Force Aero Propulsion Laboratory Research & Technology Division Air Force Systems Command United States Air Force Wright-Patterson AFB, Ohio 45433 Attn: APRP (Library)	R. Quigley C. M. Donaldson
1	Electronics Division Aerojet-General Corporation P.O. Box 296 Azusa, California 91703 Attn: Library	
1	Space General Corporation 9100 East Flair Drive El Monte, California 91734 Attn: Library	
1	Aerojet Ordnance and Manufacturing 11711 South Woodruff Avenue Fullerton, California 90241 Attn: Library	
1	Aerojet Liquid Rocket Company P. O. Box 13222 Sacramento, California 95813 Attn: Technical Library 2484-2015A	R. Stiff
1	Aeronutronic Division of Philco Ford Corp. Ford Road Newport Beach, California 92663 Attn: Technical Information Department	Dr. L. H. Linder
1	Aerospace Corporation 2400 E. El Segundo Blvd. Los Angeles, California 90045 Attn: Library-Documents	J. G. Wilder
1	Arthur D. Little, Inc. 20 Acorn Park Cambridge, Massachusetts 02140 Attn: Library	A. C. Tobey

DISTRIBUTION LIST (cont.)

Report Copies R D	Recipient	Designee
1	Astropower Laboratory McDonnell-Douglas Aircraft Company 2121 Paularino Newport Beach, California 92163 Attn: Library	
1	ARO, Incorporated Arnold Engineering Development Center Arnold AF Station, Tennessee 37389 Attn: Library	
1	Susquehanna Corporation Atlantic Research Division Shirley Highway & Edsall Road Alexandria, Virginia 22314 Attn: Library	
1	Battelle Memorial Institute 505 King Avenue Columbus, Ohio 43201 Attn: Report Library, Room 6A	
1	Beech Aircraft Corporation Boulder Facility Box 631 Boulder, Colorado Attn: Library	Douglas Pope
1 1	Bell Aerospace Company Box 1 Buffalo, New York 14240 Attn: Library	A. E. Leach
1	Bendix Systems Division Bendix Corporation 3300 Plymouth Street Ann Arbor, Michigan Attn: Library	John M. Brueger
1	Bellcomm 955 L'Enfant Plaza, S. W. Washington, D.C. Attn: Library	H. S. London

DISTRIBUTION LIST (cont.)

Report Copies R D	Recipient	Designee
1	Boeing Company Space Division P.O. Box 868 Seattle, Washington 98124 Attn: Library	J. D. Alexander C. F. Tiffany
1	Boeing Company 1625 K Street, N.W. Washington, D.C. 20006	
1	Boeing Company P.O. Box 1680 Huntsville, Alabama 35801	Ted Snow
1	Chemical Propulsion Information Agency Applied Physics Laboratory 8621 Georgia Avenue Silver Spring, Maryland 20910	Tom Reedy
1	Chrysler Corporation Missile Division P.O. Box 2628 Detroit, Michigan Attn: Library	John Gates
1	Chrysler Corporation Space Division P.O. Box 29200 New Orleans, Louisiana 70129 Attn: Librarian	
1	Grumman Aircraft Engineering Corporation Bethpage, Long Island, New York Attn: Library	Joseph Gavin
1	Hercules Powder Company Allegheny Ballistics Laboratory P.O. Box 210 Cumberland, Maryland 21501 Attn: Library	

DISTRIBUTION LIST (cont.)

Report Copies R D	Recipient	Designee
1	Honeywell, Inc. Aerospace Division 2600 Ridgeway Road Minneapolis, Minnesota Attn: Library	
1	IIT Research Institute Technology Center Chicago, Illinois 60616 Attn: Library	C. K. Hersh
1	Kidde Aer-Space Division Walter Kidde & Company, Inc. 567 Main Street Belleville, New Jersey 07109	R. J. Hanville
1	Ling-Temco-Vought Corporation P. O. Box 5907 Dallas, Texas 75222 Attn: Library	
1	Lockheed Missiles and Space Company P. O. Box 504 Sunnyvale, California 94087 Attn: Library	
1	Lockheed Propulsion Company P. O. Box 111 Redlands, California 92374 Attn: Library, Thackwell	H. L. Thackwell
1	Marquardt Corporation 16555 Saticoy Street Box 2013 - South Annex Van Nuys, California 91409	L. R. Bell, Jr.
1	Martin-Marietta Corporation (Baltimore Div.) Baltimore, Maryland 21203 Attn: Library	
1	Denver Division Martin-Marietta Corporation P. O. Box 179 Denver, Colorado 80201 Attn: Library	Dr. Morganthaler F. R. Schwartzberg

DISTRIBUTION LIST (cont.)

Report Copies R D	Recipient	Designee
1	Orlando Division Martin-Marietta Corporation Box 5827 Orlando, Florida Attn: Library	J. Fern
1	Western Division McDonnell Douglas Astronautics 5301 Bolsa Avenue Huntington Beach, California 92647 Attn: Library	R. W. Hallet G. W. Burge P. Klevatt
1	McDonnell Douglas Aircraft Corporation P. O. Box 516 Lambert Field, Missouri 63166 Attn: Library	R. A. Herzmark
1 1	Rocketdyne Division North American Rockwell, Inc. 6633 Canoga Avenue Canoga Park, California 91304 Attn: Library, Department 596-306	Donald Fulton
1	Space & Information Systems Division North American Rockwell 12214 Lakewood Blvd. Downey, California Attn: Library	
1	Northrop Space Laboratories 3401 West Broadway Hawthorne, California Attn: Library	Dr. William Howard
1	Purdue University Lafayette, Indiana 47907 Attn: Library (Technical)	Dr. Bruce Reese
1	Radio Corporation of America Astro-Electronics Products Princeton, New Jersey Attn: Library	

DISTRIBUTION LIST (cont.)

Report Copies R	D	Recipient	Designee
1		Rocket Research Corporation Willow Road at 116th Street Redmond, Washington 98052 Attn: Library	F. McCullough, Jr.
1		Standford Research Institute 333 Ravenswood Avenue Menlo Park, California 94025 Attn: Library	Dr. Gerald Marksman
1		Thiokol Chemical Corporation Redstone Division Huntsville, Alabama Attn: Library	John Goodloe
1	1	TRW Systems, Inc. 1 Space Park Redondo Beach, California 90278 Attn: Tech. Lib. Doc. Acquisitions	Curtis Watts
1		TRW TAPCO Division 23555 Euclid Avenue Cleveland, Ohio 44117	P. T. Angell
1		United Aircraft Corporation Corporation Library 400 Main Street East Hartford, Connecticut 06108 Attn: Library	Dr. David Rix Erle Martin Frank Owen Wm. E. Taylor
1	1	United Aircraft Corporation Pratt & Whitney Division Florida Research & Development Center P. O. Box 2691 West Palm Beach, Florida 33402 Attn: Library	J. P. Mitchell Dr. Schmitke
1		United Aircraft Corporation United Technology Center P. O. Box 358 Sunnyvale, California 94038 Attn: Library	Dr. David Altman

DISTRIBUTION LIST (cont.)

Report Copies R D	Recipient	Designee
1	Vickers Incorporated Box 302 Troy, Michigan	
1	Vought Astronautics Box 5907 Dallas, Texas Attn: Library	
1	Union Carbide Corporation Materials System Division 1245 Main Street Indianapolis, Indiana 46224 Attn: Library	R. L. Wolff
1	Camin Laboratories, Inc. 104-14 South Fourth Street Brooklyn, New York 11211 Attn: S. Fialkoff	